AD-430928

DISCLAIMER NOTICE

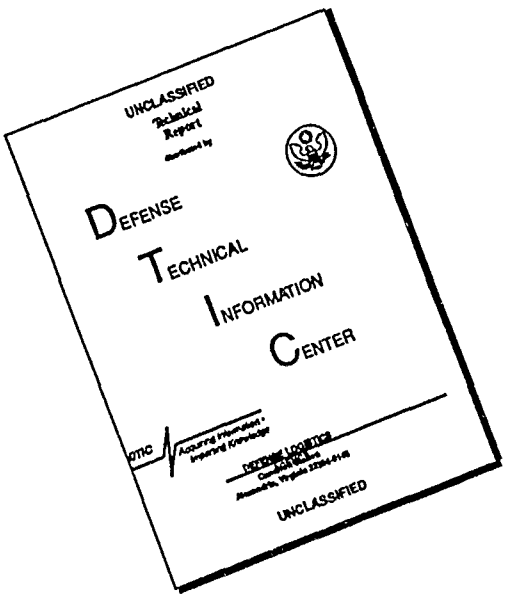

THIS DOCUMENT IS BEST QUALITY AVAILABLE. THE COPY FURNISHED TO DTIC CONTAINED A SIGNIFICANT NUMBER OF PAGES WHICH DO NOT REPRODUCE LEGIBLY.

64-9

NAVWEPS REPORT 8442
NOTS TP 3399
COPY 59

A LIFTING-SURFACE PROPELLER DESIGN METHOD FOR HIGH-SPEED COMPUTERS

by

D. M. Nelson

Underwater Ordnance Department

ABSTRACT. A propeller design method that treats the blades as lifting surfaces has been developed and programmed on an IBM 7090 computer. The singularity distributions representing the bound circulation, shed vorticity, and blade thickness are treated as continuous sheets, making it necessary to determine the Cauchy principal value of the improper integrals expressing the induced velocities on the blades. The camber lines and pitch angles are determined from the variation of the normal component of induced velocity across the blade. This method is applicable to moderately loaded, non-optimum, wake-adapted propellers with or without skew.

U.S. NAVAL ORDNANCE TEST STATION

China Lake, California

January 1964

U. S. NAVAL ORDNANCE TEST STATION

AN ACTIVITY OF THE BUREAU OF NAVAL WEAPONS

C. BLENMAN, JR., CAPT., USN
Commander

WM. B. MCLEAN, PH.D.
Technical Director

FOREWORD

This report presents the development of a propeller design method that treats the blades as lifting surfaces. The method has been programmed on an IBM 7090 computer and is available for design calculations.

The work was undertaken to make available at the U. S. Naval Ordnance Test Station the most up-to-date technique for the design of marine propellers. It was done from September 1961 to October 1963 under Bureau of Naval Weapons Task Assignment RUTO-3E-000/216-1/R009-01-03, Problem Assignment 428.

The considered opinions of the Propulsion Division are represented in this report.

Released by
J. W. HOYT, Head,
Propulsion Division
16 December 1963

Under authority of
D. J. WILCOX, Head,
Underwater Ordnance
Department

NOTS Technical Publication 3399
NAVWEPS Report 8442

Published by ..... Underwater Ordnance Department
Manuscript 807/MS-153
Collation ..... Cover, 26 leaves, abstract cards
First printing ..... 165 numbered copies
Security classification ..... UNCLASSIFIED

CONTENTS

NOMENCLATURE

C	Chord
d	Chordwise coordinate measured from leading edge (Fig. 3a)
dA	Infinitesimal area of helical sheet
$d\ell$	Infinitesimal length of vortex line element
D	Propeller diameter
f_0	$\frac{V}{v_s}\frac{C}{D}r_R$
$f_1, f_2, \ldots, f_8$	Functions of x (Eq. 10)
g	Number of blades
G	Nondimensional bound circulation
Δh	Nondimensional camber offset (Fig. 13)
k	Ratio of the strength of a line element of free vorticity at any chordwise station to that at the trailing edge
L	Distance from the stacking line to the leading edge of blade section (Fig. 3a)
r	Radial coordinate
r_R	Ratio of percent thickness of blade section at any spanwise station to percent thickness at reference station
R	Propeller radius
S	Distance from a point on one of the blades to point p
v	Local axial inflow velocity to propeller
v_s	Forward speed of propeller relative to undisturbed fluid
V	Relative velocity of blade section and fluid (Fig. 12)
W	Induced velocity
$W_{\overline{Y}}$	Normal component of induced velocity
$\Delta W_{\overline{Y}}$	Contribution to $W_{\overline{Y}}$ from the singularity region
x	Nondimensional radial coordinate (Eq. 7)
x_Δ	Nondimensional radial coordinate measured from center of chordwise strip or center of singularity region (Fig. 7, 9, 11)

X, Y, Z	Nondimensional rectangular coordinate system at propeller axis (Eq. 7)
X', Y', Z'	Rectangular coordinate system at propeller axis (Fig. 1)
$\bar{X}', \bar{Y}', \bar{Z}'$	Rectangular coordinate system on helical sheet (Fig. 2)
y	Nondimensional chordwise coordinate (Eq. 4)
y_Δ	Nondimensional chordwise coordinate measured from center of spanwise strip or center of singularity region (Fig. 4, 7)
z	Nondimensional half-thickness of blade (Fig. 12)
α	Angle defining points on helical sheets (Fig. 1)
α_Δ	Angle defining points of helical sheets measured from center of singularity region
β	Pitch angle of helical sheets (Fig. 1)
γ	Variation of pitch angle from lifting-line value
Γ	Bound circulation
$\bar{\Gamma}$	Strength of vortex line element
η	Source strength
λ	$x \tan \beta$
μ	Surface source density
ϕ	Source potential
ψ	Angle describing stacking-line locations (Fig. 1)
ω	Angular velocity of propeller

SUBSCRIPTS

B	Due to bound circulation
F	Due to free vorticity
p	Corresponding to the singularity point p
T	Due to blade thickness

INTRODUCTION

The existing marine propeller design methods that can be utilized without a high-speed computer are normally built up from optimum propeller lifting-line theory, two-dimensional slender-airfoil theory, and correction factors applied to the two-dimensional results to account for three-dimensional effects. Of these methods the most comprehensive is probably that of Eckhardt and Morgan (Ref. 1).

Since these methods are applied to non-optimum propellers of essentially arbitrary blade shape and even to wake-adapted propellers, close examination of their underlying assumptions raises some question about their ability to produce satisfactory propeller designs. For example, the induced velocities at the lifting line predicted by optimum propeller theory are positive at all spanwise stations on the blade. However, as Lerbs (Ref. 2) points out, and as is substantiated by the present work, non-optimum propellers may and normally do have rather large negative induced velocities near the hub and the tip. Also, the camber correction factors that usually have been obtained from the work of Ludwieg and Ginzel (Ref. 3 and 4) are applied to both free-running and wake-adapted propellers of arbitrary blade shape, circulation distribution, and advance ratio. Since the Ludwieg and Ginzel calculations were made for only a few cases of free-running propellers, rather crude interpolations on extrapolations are necessary. Furthermore, the pitch correction factor proposed by Lerbs (Ref. 5) and used in the Eckhardt and Morgan method is derived on the assumption that the propeller is developing lift by angle of attack and is then applied to propellers developing lift by camber. Inconsistencies such as these may be the cause of the inadequacies of these methods, because experience has shown that they do not always lead to satisfactory propeller designs, particularly when cavitation resistance is concerned.

Lack of confidence in such approximate methods has prompted a considerable amount of work in the past few years on lifting-surface theory and design methods for marine propellers. Work in the United States has been done by Pien (Ref. 6) and Kerwin (Ref. 7), in the Netherlands by Sparenberg (Ref. 8) and by van Manen and Bakker (Ref. 9), in England by Cox (Ref. 10), and in Japan by Nishiyama and Nakajima (Ref. 11). In all these studies, however, no extensive calculations were made that would permit the design of a non-optimum, wake-adapted propeller with a specified blade shape and circulation distribution. In fact, the number of parameters that would have to be varied (wake fraction, blade shape, circulation distribution, number of blades, and advance ratio) and the long computing times needed for such calcutions make such an investigation impractical. Hence, to design

propellers treating them as lifting surfaces, the facilities must be at hand to carry out the design calculations. To this end, the work described in this report was undertaken.

Propellers for torpedoes are of primary interest at the Naval Ordnance Test Station. Since these propellers operate in a wake, and since good cavitation resistance dictates circulation distributions that are not optimum, a lifting-surface design method that is applicable to non-optimum, wake-adapted propellers has been developed. This development goes one step beyond any of the works referenced above in that the effect of the blade thickness is accounted for.

REPRESENTATION OF PROPELLER SYSTEM BY SINGULARITY DISTRIBUTIONS

Each propeller blade is represented by a continuous sheet of vorticity creating the bound circulation and by a continuous sheet of sources and sinks representing the blade thickness. Since elements of vorticity cannot end in space, spanwise variations in the bound circulation give rise to elements of free or shed vorticity in the fluid that are left in helical paths along and behind the propeller. The shed vorticity for each blade is represented by a continuous helical sheet of vorticity starting at the leading edge of the blade and extending back to infinity. In this development, the hub boundary condition has been ignored and there are therefore no singularities representing the hub.

SPATIAL LOCATION OF SINGULARITIES REPRESENTING PROPELLER SYSTEM

Before the calculation of the velocities induced by the propeller can begin, the singularities representing the propeller system must be properly located in space. Lerbs' induction factor method (Ref. 2) for the lifting-line solution of the moderately loaded, non-optimum, wake-adapted propeller offers the best approximation to the spanwise pitch distribution of the helical sheets upon which the singularities representing the propeller should be located. In fact, for the free-running, unskewed, optimum or lightly loaded non-optimum propeller with negligible blade thickness, symmetrical blade shape, and symmetrical chordwise loading, the spanwise pitch distribution given by Lerbs' lifting-line solution is identical to the spanwise pitch distribution of the blade chordlines given by the lifting-surface solution. For other conditions, the pitch of the blade chordlines will usually differ only slightly from the pitch of the helical sheets given by Lerbs' lifting-line solution.

Since the object of the lifting-surface solution is to determine the camber lines, it is not possible to distribute the vorticity representing the bound circulation on the camber lines. Instead, the vorticity is distributed on the helical sheets from Lerbs' solution. This approximation is similar to the one made in two-dimensional slender-airfoil

theory in which the circulation is distributed along the chordline when the camber lines are computed. Since only small amounts of camber are needed in marine propellers to generate the desired lift, this approximation can lead to no serious error in computing the camber lines. The sources and sinks representing the blade are also distributed on the helical sheets when the effects of blade thickness are computed.

Since the free or shed vorticity in the fluid is left behind in helical paths whose pitch is determined by the relative flow of the propeller and fluid, the elements of free vorticity fall naturally on helical sheets that are very close to or identical to those given by Lerbs' lifting-line solution. Hence, when the effect of the free vorticity is computed, it is distributed on the helical sheets from Lerbs' solution.

COORDINATE SYSTEMS USED IN ANALYSIS

Figure 1 shows the coordinates used to describe the helical system upon which the singularities are distributed. The angles, ψ_m, which are given by

$$\psi_m = \frac{m-1}{g} 2\pi \qquad (m = 1, 2, \ldots, g)$$

where g is the number of blades, describe the lines where the propeller blades intersect the plane $X' = 0$. These lines are referred to as the stacking lines and are chosen coincident with the lifting lines of Lerbs' solution. For unskewed propellers they will also be chosen coincident with the line passing through the centers of lift of the blade sections.

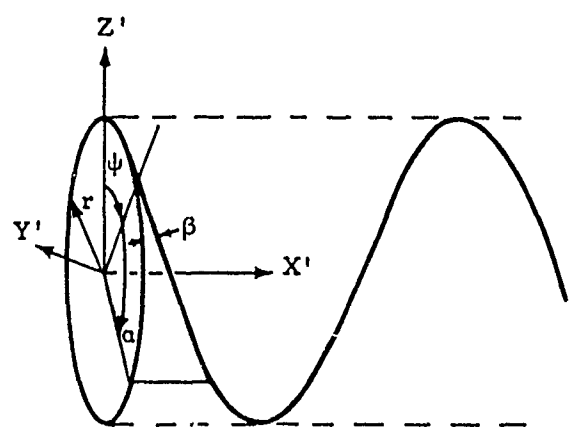

FIG. 1.

One line element at a constant radius of the helical sheet streaming back from one of the propeller stacking-line locations is shown. This element makes the pitch angle β with respect to the plane $X' = 0$. The coordinates of a point on the helical sheets in the rectangular X', Y', Z' coordinate system can then be written

$$X' = a r \tan\beta$$

$$Y' = -r \sin(\psi_m + a)$$

$$Z' = r \cos(\psi_m + a) \qquad (1)$$

Another coordinate system needed in the analysis, the rectangular $\overline{X}'$, $\overline{Y}'$, $\overline{Z}'$ system, is shown in Fig. 2. In this system the $\overline{Z}'$ axis intersects the X' axis perpendicularly, the $\overline{X}'$ axis is tangent at point p to a constant radius line element of the helical sheet streaming back from

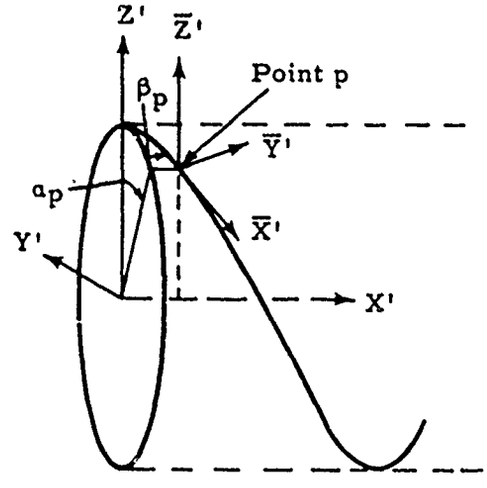

FIG. 2.

the stacking-line location $\psi_1 = 0$, and the $\overline{Y}'$ axis is normal to this line element at point p. A vector having components A_X, A_Y, A_Z in the X', Y', Z' coordinate system will have components in the $\overline{X}'$, $\overline{Y}'$, $\overline{Z}'$ coordinate system given by

$$A_{\overline{X}} = A_X \sin\beta_p - A_Y \cos a_p \cos\beta_p - A_Z \sin a_p \cos\beta_p$$

$$A_{\overline{Y}} = A_X \cos\beta_p + A_Y \cos a_p \sin\beta_p + A_Z \sin a_p \sin\beta_p$$

$$A_{\overline{Z}} = -A_Y \sin a_p + A_Z \cos a_p \qquad (2)$$

APPROACH TAKEN IN MATHEMATICS OF SOLUTION

When the velocities induced by the singularities representing the propeller system are computed, double integrals must be solved. The integrands are such that integration cannot be performed analytically with respect to either of the variables. In order to bypass the difficulty of performing numerical double integration, the region to be integrated is divided into strips sufficiently narrow that certain approximations hold accurately across them. These approximations, together with some restrictions put on the form of the circulation distribution, allow integration to be performed across the strips analytically. Thus, instead of a numerical double integration there is an analytical integration across the strip, a numerical integration along the strip, and a summation over the strips. This process is applied everywhere except in a small region around the point where the velocity is desired, since a singularity occurs in the integrand at that point, making numerical integration through the point impossible. Integration is carried out analytically over this small singularity region to obtain the Cauchy principal value. To make an analytical integration possible over this region, several approximations were necessary which in essence amount to (1) assuming a linear variation of most of the variables over the region, plus (2) discarding third and higher-order terms in the small nondimensional coordinates describing the distance of a point from the singularity point. The check solutions run to date showed that the region may be chosen sufficiently small that these approximations yield a good value of the contribution of the region to the velocity, without being so small that the numerical integration in the area immediately surrounding the region cannot be carried out accurately.

An important feature of this approach is that the point where the velocity is desired, i.e., the singularity point, is always chosen at the center of the strips and at the centroid of the small region surrounding the singularity. Also, all approximations are expanded about the center of the strips or the centroid of the singularity region. By doing this, the accuracy of the method is greatly enhanced and computing times are reduced since the number of points needed to obtain an accurate numerical integration is smaller.

Two restrictions, mentioned above, were placed on the circulation distribution to facilitate integration across the strips: (1) the chordwise distribution of circulation must be made up of straight line segments, and (2) the spanwise distribution of circulation must lend itself to an accurate piecewise approximation by parabolic sections. Since fairly optimum chordwise distributions of circulation from the standpoint of cavitation resistance can be made up of straight line segments, and since most practical spanwise circulation distributions do not have extremely large third derivatives, these restrictions offer no serious restriction on the generality of the method.

DESIRED COMPONENT OF INDUCED VELOCITY

Because the component of induced velocity parallel to the blade-section chordline will normally be very small compared to the relative velocity of the blade section and the still fluid, it may be neglected in the boundary condition when the camber lines are being determined. Only the component of induced velocity normal to the blade-section chordline is needed to determine the camber-line boundary condition. This approximation is identical to that used in slender-airfoil theory. Assuming that all induced velocities are to be computed on the blade $\psi_1 = 0$, the normal component of induced velocity, denoted by $W_{\bar{Y}}$, will be in the $\bar{Y}'$ direction shown in Fig. 2. There are three contributions to $W_{\bar{Y}}$: the one resulting from the bound circulation $(W_{\bar{Y}})_B$, the one resulting from the free vorticity, $(W_{\bar{Y}})_F$, and the one resulting from the blade thickness $(W_{\bar{Y}})_T$. Hence,

$$W_{\bar{Y}} = (W_{\bar{Y}})_B + (W_{\bar{Y}})_F + (W_{\bar{Y}})_T \tag{3}$$

CALCULATION OF NORMAL COMPONENT OF INDUCED VELOCITY

VELOCITY DUE TO BOUND CIRCULATION $(W_{\bar{Y}})_B$

The position of points on a blade section are shown in Fig. 3a, where C is the chord, d is the distance from the leading edge, and L is the

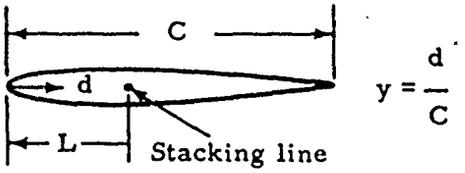

FIG. 3a.

distance from the stacking line to the leading edge. A nondimensional chordwise coordinate is defined as

$$y = \frac{d}{C} \tag{4}$$

The location of each vortex line element of the bound circulation sheet is given by the condition y = Constant, as illustrated in Fig. 3b for an unskewed propeller and in Fig. 3c for a skewed propeller. This choice of the location of an element of the bound circulation sheet is the most convenient one, since elements of free or shed vorticity arise only from a change in the spanwise distribution of circulation. For the other methods of locating the elements of the bound circulation sheet,

(Blade shown flat here and in following sketches to simplify drawing)

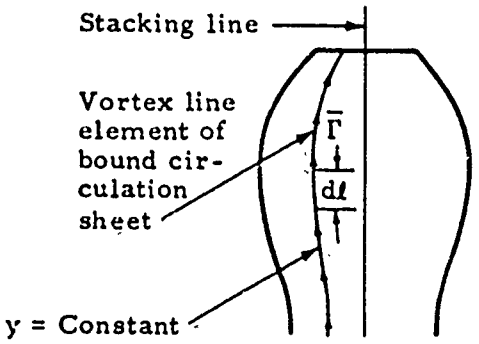

Unskewed Propeller

FIG. 3b.

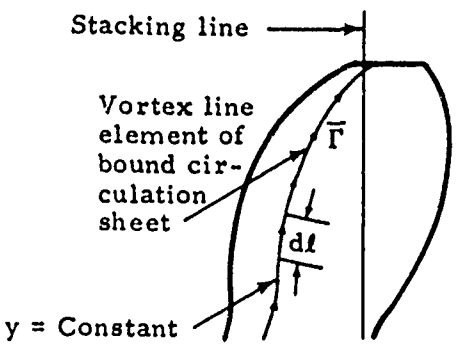

Skewed Propeller

FIG. 3c.

such as that shown in Fig. 3d, elements of shed vorticity arise not only from a change in the spanwise distribution of circulation but also as a result of blade taper. The added complication of having to consider both these effects in the calculations involving the free vorticity make such a method impractical.

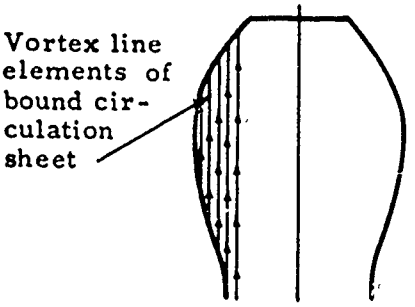

Impractical Representation of Bound Circulation

FIG. 3d.

Referring to Fig. 1 and measuring the distances d and L_t along the constant radius helical line with the stacking line in the plane $X' = 0$, the following relation is obtained between a and y and r.

$$a = y \frac{C \cos\beta}{r} - \frac{L \cos\beta}{r}$$

This relationship maps the propeller blades onto the helical sheets. Substituting this relationship into Eq. 1 yields the coordinates in the X', Y', Z' system of points on the blades.

$$X' = yC \sin\beta - L \sin\beta$$

$$Y' = -r \sin\left(\psi_m + y\frac{C\cos\beta}{r} - \frac{L\cos\beta}{r}\right)$$

$$Z' = r\cos\left(\psi_m + y\frac{C\cos\beta}{r} - \frac{L\cos\beta}{r}\right) \qquad (5)$$

Letting $d\ell$ be an infinitesimal length of a vortex line element making up the bound circulation sheet, as illustrated in Fig. 3b and 3c, the components of $d\ell$ in the X', Y', Z' system are obtained with Eq. 5 as follows.

$$\frac{d\ell_X}{dr} = \left.\frac{dX'}{dr}\right|_{y=\text{Constant}}$$

$$\frac{d\ell_X}{dr} = y\frac{d(C\sin\beta)}{dr} - \frac{d(L\sin\beta)}{dr}$$

$$\frac{d\ell_Y}{dr} = \left.\frac{dY'}{dr}\right|_{y=\text{Constant}}$$

$$\frac{d\ell_Y}{dr} = -\cos\left(\psi_m + y\frac{C\cos\beta}{r} - \frac{L\cos\beta}{r}\right)\left\{y\left[\frac{d(C\cos\beta)}{dr} - \frac{C\cos\beta}{r}\right] - \left[\frac{d(L\cos\beta)}{dr} - \frac{L\cos\beta}{r}\right]\right\} - \sin\left(\psi_m + y\frac{C\cos\beta}{r} - \frac{L\cos\beta}{r}\right)$$

$$\frac{d\ell_Z}{dr} = \left.\frac{dZ'}{dr}\right|_{y=\text{Constant}}$$

$$\frac{d\ell_Z}{dr} = -\sin\left(\psi_m + y\frac{C\cos\beta}{r} - \frac{L\cos\beta}{r}\right)\left\{y\left[\frac{d(C\cos\beta)}{dr} - \frac{C\cos\beta}{r}\right] - \left[\frac{d(L\cos\beta)}{dr} - \frac{L\cos\beta}{r}\right]\right\} + \cos\left(\psi_m + y\frac{C\cos\beta}{r} - \frac{L\cos\beta}{r}\right)$$

Letting the subscript p denote the point p where the normal component of velocity is desired, and remembering that all velocities are to be computed on the blade $\psi_1 = 0$, the coordinates in the X', Y', Z' system of the point p are, from Eq. 5,

$$X'_p = y_p(C \sin\beta)_{r=r_p} - (L \sin\beta)_{r=r_p}$$

$$Y'_p = -r_p \sin a_p$$

$$Z'_p = r_p \cos a_p \tag{6}$$

where

$$a_p = y_p\left(\frac{C \cos\beta}{r}\right)_{r=r_p} - \left(\frac{L \cos\beta}{r}\right)_{r=r_p}$$

The X', Y', Z' components of the distance, S, from an element of vorticity on one of the blades to the point p are obtained from Eq. 5 and 6.

$$S_X = X'_p - yC \sin\beta + L \sin\beta$$

$$S_Y = Y'_p + r \sin\left(\psi_m + y\frac{C \cos\beta}{r} - \frac{L \cos\beta}{r}\right)$$

$$S_Z = Z'_p - r \cos\left(\psi_m + y\frac{C \cos\beta}{r} - \frac{L \cos\beta}{r}\right)$$

Nondimensionalizing with the propeller radius, R, and diameter, D, and introducing the nondimensional coordinates,

$$x = \frac{r}{R}, \quad X = \frac{X'}{R}, \quad Y = \frac{Y'}{R}, \quad Z = \frac{Z'}{R} \tag{7}$$

the components of $d\ell$ and S may be written

$$\frac{d\ell_X}{Rdx} = yf_5 - f_6$$

$$\frac{d\ell_Y}{Rdx} = -\cos(\psi_m + yf_3 - f_4)[y(f_7 - f_3) - (f_8 - f_4)] - \sin(\psi_m + yf_3 - f_4)$$

$$\frac{d\ell_Z}{Rdx} = -\sin(\psi_m + yf_3 - f_4)[y(f_7 - f_3) - (f_8 - f_4)] + \cos(\psi_m + yf_3 - f_4)$$

$$\frac{S_X}{R} = X_p - yf_1 + f_2$$

$$\frac{S_Y}{R} = Y_p + x \sin(\psi_m + yf_3 - f_4)$$

$$\frac{S_Z}{R} = Z_p - x \cos(\psi_m + yf_3 - f_4) \tag{8}$$

where

$$X_p = y_p f_{1p} - f_{2p}$$
$$Y_p = -x_p \sin a_p$$
$$Z_p = x_p \cos a_p$$
$$a_p = y_p f_{3p} - f_{4p} \tag{9}$$

and where

$$f_1 = 2\frac{C}{D}\sin\beta, \qquad f_{1p} = (f_1)_{x=x_p}$$

$$f_2 = 2\frac{L}{D}\sin\beta, \qquad f_{2p} = (f_2)_{x=x_p}$$

$$f_3 = \frac{2(C/D)\cos\beta}{x}, \qquad f_{3p} = (f_3)_{x=x_p}$$

$$f_4 = \frac{2(L/D)\cos\beta}{x}, \qquad f_{4p} = (f_4)_{x=x_p}$$

$$f_5 = \frac{d[2(C/D)\sin\beta]}{dx}, \qquad f_{5p} = (f_5)_{x=x_p}$$

$$f_6 = \frac{d[2(L/D)\sin\beta]}{dx}, \qquad f_{6p} = (f_6)_{x=x_p}$$

$$f_7 = \frac{d[2(C/D)\cos\beta]}{dx}, \qquad f_{7p} = (f_7)_{x=x_p}$$

$$f_8 = \frac{d[2(L/D)\cos\beta]}{dx}, \qquad f_{8p} = (f_8)_{x=x_p} \tag{10}$$

Breaking the blade into spanwise strips bounded by lines y = Constant, as illustrated in Fig. 4, there may be written for each strip

$$y = \bar{y}_n + \bar{y}_\Delta \tag{11}$$

The subscript n takes on the values 1, 2, 3, ... , s, where s is the number of strips. Substituting Eq. 11 into Eq. 8, using the trigonometric

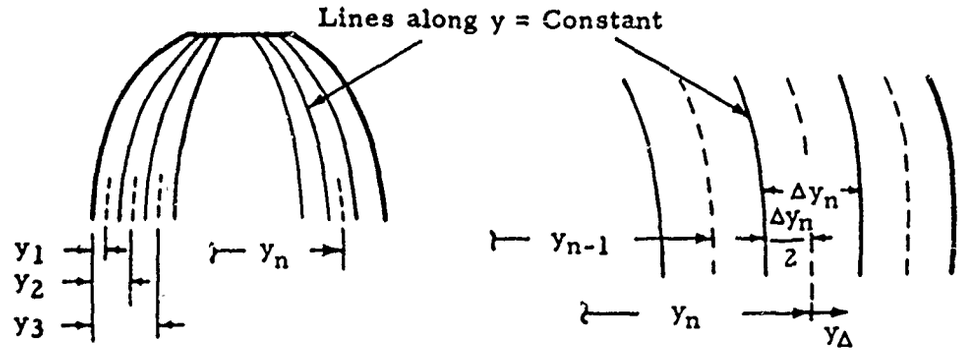

FIG. 4.

identities for the sin and cos of the sum of two angles, and restricting the maximum half-width of the strips, $(y_\Delta)_{max} = (\Delta y_n/2)_{max}$ so that

$$\cos(y_\Delta f_3)_{max} \cong 1, \qquad \sin(y_\Delta f_3)_{max} \cong (y_\Delta f_3)_{max} \tag{12}$$

the expressions for the components of $d\ell$ and S in the X', Y', Z' coordinate system become

$$\frac{d\ell_X}{R dx} = y_n f_5 - f_6 + f_5 y_\Delta$$

$$\frac{d\ell_Y}{R dx} = [f_8 - f_4 - y_n(f_7 - f_3)]\cos(\psi_m + y_n f_3 - f_4) - \sin(\psi_m + y_n f_3 - f_4)$$
$$- \{[f_8 - f_4 - y_n(f_7 - f_3)]f_3 \sin(\psi_m + y_n f_3 - f_4) + f_7 \cos(\psi_m + y_n f_3 - f_4)\} y_\Delta$$
$$+ f_3(f_7 - f_3)\sin(\psi_m + y_n f_3 - f_4) y_\Delta^2$$

$$\frac{d\ell_Z}{R dx} = [f_8 - f_4 - y_n(f_7 - f_3)]\sin(\psi_m + y_n f_3 - f_4) + \cos(\psi_m + y_n f_3 - f_4)$$
$$+ \{[f_8 - f_4 - y_n(f_7 - f_3)]f_3 \cos(\psi_m + y_n f_3 - f_4) - f_7 \sin(\psi_m + y_n f_3 - f_4)\} y_\Delta$$
$$- f_3(f_7 - f_3)\cos(\psi_m + y_n f_3 - f_4) y_\Delta^2$$

$$\frac{S_X}{R} = X_p + x \cos(\psi_m + y_n f_3 - f_4) - x f_3 \sin(\psi_m + y_n f_3 - f_4) y_\Delta$$

$$\frac{S_Y}{R} = Y_p + x \sin(\psi_m + y_n f_3 - f_4) + x f_3 \cos(\psi_m + y_n f_3 - f_4) y_\Delta$$

$$\frac{S_Z}{R} = Z_p - x \cos(\psi_m + y_n f_3 - f_4) + x f_3 \sin(\psi_m + y_n f_3 - f_4) y_\Delta \qquad (13)$$

The Biot-Savart law is used to compute the induced velocity due to the vorticity representing the bound circulation. This law is stated

$$\vec{W} = \frac{1}{4\pi} \int_l \overline{\Gamma} \frac{\vec{dl} \times \vec{S}}{S^3} \qquad (14)$$

where dl is an infinitesimal length of an element of vorticity, S is the distance from the element of vorticity to the point where the velocity, W, is desired, and $\overline{\Gamma}$ is the strength of the vortex element. Since only the normal component of W, i.e., $W_{\overline{Y}}$, is desired, there is obtained from Eq. 14

$$W_{\overline{Y}} = \frac{1}{4\pi} \int_l \overline{\Gamma} \frac{S_{\overline{X}} dl_{\overline{Z}} - S_{\overline{Z}} dl_{\overline{X}}}{S^3} \qquad (15)$$

The strength, $\overline{\Gamma}$, of the vortex element as a function of the spanwise and chordwise distribution of bound circulation is determined as follows. Specify a spanwise distribution of bound circulation, Γ, extending from the hub, $x = x_h$, to the tip, $x = 1$, as illustrated in Fig. 5. Assuming

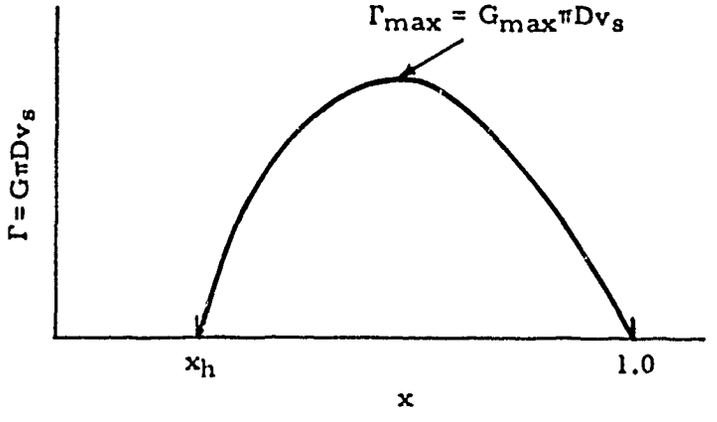

FIG. 5.

that the shape of the chordwise loading is independent of spanwise position, it is necessary to specify it at only one position. Thus, specify a chordwise distribution of bound circulation at the spanwise position $\Gamma = \Gamma_{max}$, as shown in Fig. 6.

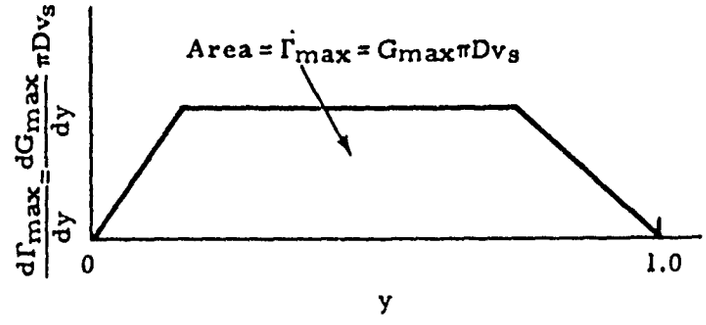

FIG. 6.

The strength, $\overline{\Gamma}$, may then be written

$$\overline{\Gamma} = \frac{\Gamma}{\Gamma_{max}} \frac{d\Gamma_{max}}{dy} dy$$

Nondimensionalizing the bound circulation using the propeller diameter, D, and the forward velocity of the propeller relative to the undisturbed fluid, v_s,

$$G = \frac{\Gamma}{\pi Dv_s}$$

the expression for $\overline{\Gamma}$ becomes

$$\frac{\overline{\Gamma}}{\pi Dv_s} = \frac{G}{G_{max}} \frac{dG_{max}}{dy} dy \tag{16}$$

Restricting the chordwise distribution of bound circulation to one that can be made up of straight line segments, as discussed previously, Eq. 16 may be written for each spanwise strip

$$\frac{\overline{\Gamma}}{\pi Dv_s} = \frac{G}{G_{max}} \left[\left(\frac{dG_{max}}{dy} \right)_{y=y_n} + \left(\frac{d^2 G_{max}}{dy^2} \right)_{y=y_n} y_\Delta \right] dy_\Delta \tag{17}$$

Equation 2 allows the components of $d\ell$ and S in the $\overline{X}'$, $\overline{Y}'$, $\overline{Z}'$ system to be determined from their components in the X', Y', Z' system,

given by Eq. 13. Substituting these $\bar{X}'$, $\bar{Y}'$, $\bar{Z}'$ components into Eq. 15 and using Eq. 17, the expression for the normal component of induced velocity due to the bound circulation becomes

$$\frac{(W_{\bar{Y}})_B}{v_s} = \frac{1}{2} \sum_{m=1}^{g} \sum_{n=1}^{s} \int_{xh}^{1} \frac{G}{G_{max}} \int_{-\Delta y_n/2}^{\Delta y_n/2} \frac{A_0 H_n + (A_0 K_n + A_1 H_n) y_\Delta + (A_1 K_n + A_2 H_n) y_\Delta^2 + (A_2 K_n + A_3 H_n) y_\Delta^3 + A_3 K_n y_\Delta^4}{(a + b y_\Delta + c y_\Delta^2)^{3/2}} dy_\Delta dx \tag{18}$$

where

$$H_n = \left(\frac{dG_{max}}{dy}\right)_{y=y_n}$$

$$K_n = \left(\frac{d^2 G_{max}}{dy^2}\right)_{y=y_n}$$

$$a = 2Y_p x \sin(\psi_m + y_n f_3 - f_4) - 2Z_p x \cos(\psi_m + y_n f_3 - f_4) + (X_p - y_n f_1 + f_2)^2 + Y_p^2 + Z_p^2 + x^2$$

$$b = 2Y_p x f_3 \cos(\psi_m + y_n f_3 - f_4) + 2Z_p x f_3 \sin(\psi_m + y_n f_3 - f_4) - 2f_1(X_p - y_n f_1 + f_2)$$

$$c = x^2 f_3^2 + f_1^2$$

$$A_0 = \{[f_8 - f_4 - y_n(f_7 - f_3)](X_p - y_n f_1 + f_2)\sin(\psi_m + y_n f_3 - f_4 - a_p) + Y_p(y_n f_5 - f_6)\sin a_p$$
$$+ [X_p - y_n f_1 + f_2 + x(y_n f_5 - f_6)]\cos(\psi_m + y_n f_3 - f_4 - a_p) - Z_p(y_n f_5 - f_6)\cos a_p\}\sin\beta_p$$
$$- \{\{Y_p[f_8 - f_4 - y_n f_7 - f_3)] + Z_p\}\sin(\psi_m + y_n f_3 - f_4) - \{Z_p[f_8 - f_4 - y_n(f_7 - f_3)] - Y_p\}$$
$$\cos(\psi_m + y_n f_3 - f_4) + x[f_8 - f_4 - y_n(f_7 - f_3)]\}\cos\beta_p$$

$$A_1 = -\{\{f_7(X_p - y_n f_1 + f_2) + f_1[f_8 - f_4 - y_n(f_7 - f_3)] + x f_3(y_n f_5 - f_6)\}\sin(\psi_m + y_n f_3 - f_4 - a_p)$$
$$- \{[f_8 - f_4 - y_n(f_7 - f_3)]f_3(X_p - y_n f_1 + f_2) - f_1 + x f_5\}\cos(\psi_m + y_n f_3 - f_4 - a_p)$$
$$- Y_p f_5 \sin a_p + Z_p f_5 \cos a_p\}\sin\beta_p$$
$$- \{\{Y_p[f_8 - f_4 - y_n(f_7 - f_3)]f_3 + Z_p f_7\}\cos(\psi_m + y_n f_3 - f_4)$$
$$+ \{Z_p[f_8 - f_4 - y_n(f_7 - f_3)]f_3 - Y_p f_7\}\sin(\psi_m + y_n f_3 - f_4) - x(f_7 - f_3)\}\cos\beta_p$$

$$A_2 = -\Big\{\big\{[f_8-f_4-y_n(f_7-f_3)]f_1f_3+(f_7-f_3)f_3(X_p-y_nf_1+f_2)\big\}\cos(\psi_m+y_nf_3-f_4-\alpha_p)$$

$$-(f_1f_7 - xf_3f_5)\sin(\psi_m + y_nf_3 - f_4 - \alpha_p)\Big\}\sin\beta_p$$

$$+\big\{f_3(f_7-f_3)[Y_p\cos(\psi_m+y_nf_3-f_4)+Z_p\sin(\psi_m+y_nf_3-f_4)]$$

$$-x[f_8-f_4-y_n(f_7-f_3)]f_3^2\big\}\cos\beta_p$$

$$A_3 = f_1f_3(f_7-f_3)\cos(\psi_m+y_nf_3-f_4-\alpha_p)\sin\beta_p+xf_3^2(f_7-f_3)\cos\beta_p$$

The integration with respect to y_Δ in Eq. 18 may be carried out analytically. The integration with respect to x must be carried out numerically. Performing the integration with respect to y_Δ, and since the numerical integration with respect to x cannot be carried through the singularity, Eq. 18 becomes

$$\frac{(W\bar{Y})_B}{v_s} = \frac{1}{2}\sum_{m=1}^{g}\sum_{n=1}^{s}\left(\int_{x_h}^{x_p-\epsilon}\frac{G}{G_{max}}Q\,dx + \int_{x_p+\epsilon}^{1}\frac{G}{G_{max}}Q\,dx\right) + \frac{(\Delta W\bar{Y})_B}{v_s} \qquad (19)$$

where

$$\epsilon = 0 \text{ for } m \neq 1 \quad \text{or} \quad y_n \neq y_p$$

$$\epsilon = \frac{\Delta x}{2} \text{ for } m = 1 \quad \text{and} \quad y_n = y_p$$

*For $|4ac - b^2| > 0.00001$

$$Q = \frac{A_3K_n}{2c}\left[\frac{y_\Delta^3}{(a + by_\Delta + cy_\Delta^2)^{1/2}}\right]_{-\Delta y_n/2}^{\Delta y_n/2}$$

$$+\frac{A_2K_n + A_3\left(H_n - K_n\frac{5b}{4c}\right)}{c}\left[\frac{y_\Delta^2}{(a + by_\Delta + cy_\Delta^2)^{1/2}}\right]_{-\Delta y_n/2}^{\Delta y_n/2}$$

$$+\frac{A_1K_n + A_2\left(H_n - K_n\frac{3b}{2c}\right) - A_3\left[H_n\frac{3b}{2c} - K_n\left(\frac{15b^2}{8c^2} - \frac{3a}{2c}\right)\right]}{c(4ac - b^2)}$$

$$\left[\frac{(2b^2 - 4ac)y_\Delta + 2ab}{(a + by_\Delta + cy_\Delta^2)^{1/2}}\right]_{-\Delta y_n/2}^{\Delta y_n/2}$$

*See footnote on next page.

$$+\frac{A_1K_n + A_2\left(H_n - K_n\frac{3b}{2c}\right) - A_3\left[H_n\frac{3b}{2c} - K_n\left(\frac{15b^2}{8c^2} - \frac{3a}{2c}\right)\right]}{c^{3/2}}$$

$$\left\{\ln\left[(a + by_\Delta + cy_\Delta^2)^{1/2} + \sqrt{c}y_\Delta + \frac{b}{2\sqrt{c}}\right]\right\}_{-\Delta y_n/2}^{\Delta y_n/2}$$

$$-\frac{2\left[A_0K_n + A_1H_n - A_2K_n\frac{2a}{c} - A_3\left(H_n\frac{2a}{c} - K_n\frac{10ab}{4c^2}\right)\right]}{4ac - b^2}$$

$$\left[\frac{by_\Delta + 2a}{(a + by_\Delta + cy_\Delta^2)^{1/2}}\right]_{-\Delta y_n/2}^{\Delta y_n/2} + \frac{2A_0H_n}{4ac - b^2}\left[\frac{2cy_\Delta + b}{(a + by_\Delta + cy_\Delta^2)^{1/2}}\right]_{-\Delta y_n/2}^{\Delta y_n/2}$$

*For $|4ac - b^2| \leqslant 0.00001$

$$Q = \frac{A_3K_n\sqrt{a}}{bc^2}\left[\left(\sqrt{a} + \frac{b}{2\sqrt{a}}y_\Delta\right)^2\right]_{-\Delta y_n/2}^{\Delta y_n/2}$$

$$+\frac{A_2K_n + A_3\left(H_n - K_n\frac{8a}{b}\right)}{c^2}\left(\sqrt{a} + \frac{b}{2\sqrt{a}}y_\Delta\right)_{-\Delta y_n/2}^{\Delta y_n/2}$$

$$+\frac{A_1K_n\frac{2\sqrt{a}}{b} + A_2\left(H_n\frac{2\sqrt{a}}{b} - K_n\frac{3\sqrt{a}}{c}\right) - A_3\left(H_n\frac{3\sqrt{a}}{c} - K_n\frac{12a^{3/2}}{bc}\right)}{c}$$

$$\left[\ln\left(\sqrt{a} + \frac{b}{2\sqrt{a}}y_\Delta\right)\right]_{-\Delta y_n/2}^{\Delta y_n/2}$$

---

*Under certain circumstances when $x=x_p$, $4ac - b^2 = 0$ (exactly or within the accuracy of the computer). The solution takes a different form at this point. Due to machine accuracy, the test is made on a small finite quantity rather than on zero.

$$-\frac{A_0K_n + A_1\left(H_n - K_n\frac{4a}{b}\right) - A_2\left(H_n\frac{4a}{b} - K_n\frac{3a}{c}\right) + A_3\left(H_n\frac{3a}{c} - K_n\frac{8a^2}{bc}\right)}{c}$$

$$\left(\frac{1}{\frac{b}{\sqrt{a}} + \frac{b}{2\sqrt{a}}y_\Delta}\right)\Bigg|_{-\Delta y_n/2}^{\Delta y_n/2}$$

$$-\left[A_0\left(H_n\frac{\sqrt{a}}{b} - K_n\frac{\sqrt{a}}{2c}\right) - A_1\left(H_n\frac{\sqrt{a}}{2c} - K_n\frac{a^{3/2}}{bc}\right) + A_2\left(H_n\frac{a^{3/2}}{bc} - K_n\frac{a^{3/2}}{2c^2}\right)\right.$$

$$\left. - A_3\left(H_n\frac{a^{3/2}}{2c^2} - K_n\frac{a^{5/2}}{bc^2}\right)\right]\left[\frac{1}{\left(\sqrt{a} + \frac{b}{2\sqrt{a}}y_\Delta\right)^2}\right]_{-\Delta y_n/2}^{\Delta y_n/2}$$

and where $(\Delta W\bar{Y})_B$ is the contribution to $(W\bar{Y})_B$ from the small region surrounding the singularity. The determination of $(\Delta W\bar{Y})_B$ follows.

Figure 7 shows the small region surrounding the singularity lying on the blade $\psi_1 = 0$ and having its center at the point $y_n = y_p$. The location of points within this region are given by the nondimensional coordinates y_Δ and x_Δ.

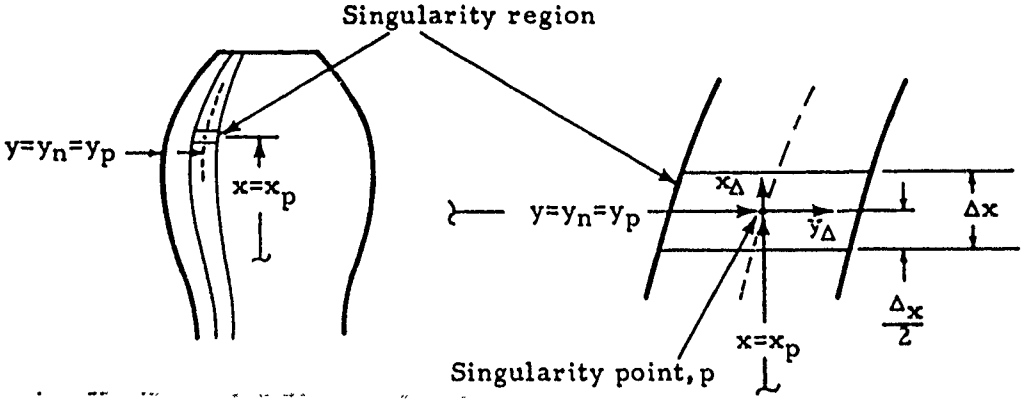

FIG. 7.

Since these coordinates are nondimensionalized with the chord and propeller radius respectively, they are very small compared to one. The nondimensional coordinates in the X', Y', Z' system of points on the blade $\psi_1 = 0$ are, from Eq. 5, 7, and 10,

$$X = yf_1 - f_2$$

$$Y = -x \sin(yf_3 - f_4)$$

$$Z = x \cos(yf_3 - f_4) \tag{20}$$

In the region surrounding the singularity,

$$x = x_p + x_\Delta$$

Assuming a linear variation of the functions of x over the region, the expressions for f_{1-4} are

$$f_1 = f_{1p} + f_{5p} x_\Delta$$

$$f_2 = f_{2p} + f_{6p} x_\Delta$$

$$f_3 = f_{3p} + (f_{7p} - f_{3p}) \frac{x_\Delta}{x_p}$$

$$f_4 = f_{4p} + (f_{8p} - f_{4p}) \frac{x_\Delta}{x_p}$$

where the f_{1-8p} are defined by Eq. 10. Substituting these expressions into Eq. 20 and utilizing the trigonometric identities for the sin and cos of the sum of angles, there is obtained

$$X = yf_{1p} - f_{2p} + (yf_{5p} - f_{6p})x_\Delta$$

$$Y = -(x_p + x_\Delta)\sin(yf_{3p} - f_{4p})\cos\left\{[y(f_{7p} - f_{3p}) - (f_{8p} - f_{4p})]\frac{x_\Delta}{x_p}\right\}$$

$$- (x_p + x_\Delta)\cos(yf_{3p} - f_{4p})\sin\left\{[y(f_{7p} - f_{3p}) - (f_{8p} - f_{4p})]\frac{x_\Delta}{x_p}\right\}$$

$$Z = (x_p + x_\Delta)\cos(yf_{3p} - f_{4p})\cos\left\{[y(f_{7p} - f_{3p}) - (f_{8p} - f_{4p})]\frac{x_\Delta}{x_p}\right\}$$

$$- (x_p + x_\Delta)\sin(yf_{3p} - f_{4p})\sin\left\{[y(f_{7p} - f_{3p}) - (f_{8p} - f_{4p})]\frac{x_\Delta}{x_p}\right\} \tag{21}$$

Restricting $(x_\Delta/x_p)_{max} = \Delta x/2x_p$ to be very small compared to one, so that

$$*\sin\left\{\left[y(f_{7p} - f_{3p}) - (f_{8p} - f_{4p})\right]\frac{x_\Delta}{x_p}\right\}_{max} \cong \left\{\left[y(f_{7p} - f_{3p}) - (f_{8p} - f_{4p})\right]\frac{x_\Delta}{x_p}\right\}_{max}$$

$$\cos\left\{\left[y(f_{7p} - f_{3p}) - (f_{8p} - f_{4p})\right]\frac{x_\Delta}{x_p}\right\}_{max} \cong 1$$

$$1 + \left(\frac{x_\Delta}{x_p}\right)_{max} \cong 1 \qquad (22)$$

Equation 21 becomes

$$X = yf_{1p} - f_{2p} + (yf_{5p} - f_{6p})x_\Delta$$

$$Y = -x_p \sin(yf_{3p} - f_{4p}) - \left\{\sin(yf_{3p} - f_{4p}) + \cos(yf_{3p} - f_{4p})\left[y(f_{7p} - f_{3p}) - (f_{8p} - f_{4p})\right]\right\}x_\Delta$$

$$Z = x_p \cos(yf_{3p} - f_{4p}) + \left\{\cos(yf_{3p} - f_{4p}) - \sin(yf_{3p} - f_{4p})\left[y(f_{7p} - f_{3p}) - (f_{8p} - f_{4p})\right]\right\}x_\Delta \qquad (23)$$

Introducing again the expression for y within a strip,

$$y = y_n + y_\Delta = y_p + y_\Delta$$

using the trigonometric identities for the sin and cos of the sum of angles, and remembering the restriction that has been made concerning $(y_\Delta f_3)_{max}$ (see Eq. 12), Eq. 23 becomes

$$X = y_p f_{1p} - f_{2p} + f_{1p}y_\Delta + f_{5p}y_\Delta x_\Delta + (y_p f_{5p} - f_{6p})x_\Delta$$

$$Y = -x_p \sin a_p - x_p f_{3p} \cos a_p y_\Delta - f_{3p}\left\{\cos a_p - \sin a_p\left[(y_p + y_\Delta)(f_{7p} - f_{3p}) - (f_{8p} - f_{4p})\right]\right\}y_\Delta x_\Delta - \left\{\sin a_p + \cos a_p\left[(y_p + y_\Delta)(f_{7p} - f_{3p}) - (f_{8p} - f_{4p})\right]\right\}x_\Delta$$

$$Z = x_p \cos a_p - x_p f_{3p} \sin a_p y_\Delta - f_{3p}\left\{\sin a_p + \cos a_p\left[(y_p + y_\Delta)(f_{7p} - f_{3p}) - (f_{8p} - f_{4p})\right]\right\}y_\Delta x_\Delta + \left\{\cos a_p - \sin a_p\left[(y_p + y_\Delta)(f_{7p} - f_{3p}) - (f_{8p} - f_{4p})\right]\right\}x_\Delta \qquad (24)$$

*These approximations imply certain restrictions on f_7 and f_8 which are discussed later.

Using Eq. 24 and 9, the expressions for the components of $d\ell$ and S in the X', Y', Z' coordinate system are easily obtained.

$$\frac{d\ell_X}{dx_\Delta} = \frac{dX'}{dx_\Delta}\bigg|_{y_\Delta=\text{Constant}} = R\frac{dX}{dx_\Delta}\bigg|_{y_\Delta=\text{Constant}}$$

$$\frac{d\ell_X}{R dx_\Delta} = y_p f_{5p} - f_{6p} + f_{5p} y_\Delta$$

$$\frac{d\ell_Y}{dx_\Delta} = \frac{dY'}{dx_\Delta}\bigg|_{y_\Delta=\text{Constant}} = R\frac{dY}{dx_\Delta}\bigg|_{y_\Delta=\text{Constant}}$$

$$\frac{d\ell_Y}{R dx_\Delta} = -\sin a_p - \cos a_p[(y_p + y_\Delta)(f_{7p} - f_{3p}) - (f_{8p} - f_{4p})]$$
$$-f_{3p}\{\cos a_p - \sin a_p[(y_p + y_\Delta)(f_{7p} - f_{3p}) - (f_{8p} - f_{4p})]\} y_\Delta$$

$$\frac{d\ell_Z}{dx_\Delta} = \frac{dZ'}{dx_\Delta}\bigg|_{y_\Delta=\text{Constant}} = R\frac{dZ}{dx_\Delta}\bigg|_{y_\Delta=\text{Constant}}$$

$$\frac{d\ell_Z}{R dx_\Delta} = \cos a_p - \sin a_p[(y_p + y_\Delta)(f_{7p} - f_{3p}) - (f_{8p} - f_{4p})]$$
$$-f_{3p}\{\sin a_p + \cos a_p[(y_p + y_\Delta)(f_{7p} - f_{3p}) - (f_{8p} - f_{4p})]\} y_\Delta$$

$$S_X = X'_p - X' = R(X_p - X)$$

$$\frac{S_X}{R} = -f_{1p} y_\Delta - f_{5p} y_\Delta x_\Delta - (y_p f_{5p} - f_{6p}) x_\Delta$$

$$S_Y = Y'_p - Y' = R(Y_p - Y)$$

$$\frac{S_Y}{R} = x_p f_{3p} \cos a_p y_\Delta + f_{3p}\{\cos a_p - \sin a_p[(y_p + y_\Delta)(f_{7p} - f_{3p}) - (f_{8p} - f_{4p})]\} y_\Delta x_\Delta$$
$$+ \{\sin a_p + \cos a_p[(y_p + y_\Delta)(f_{7p} - f_{3p}) - (f_{8p} - f_{4p})]\} x_\Delta$$

$$S_Z = Z'_p - Z' = R(Z_p - Z)$$

$$\frac{S_Z}{R} = x_p f_{3p} \sin a_p y_\Delta + f_{3p}\{\sin a_p + \cos a_p[(y_p + y_\Delta)(f_{7p} - f_{3p}) - (f_{8p} - f_{4p})]\} y_\Delta x_\Delta$$
$$- \{\cos a_p - \sin a_p[(y_p + y_\Delta)(f_{7p} - f_{3p}) - (f_{8p} - f_{4p})]\} x_\Delta \quad (25)$$

Making a linear approximation in Eq. 17 to the bound circulation across the singularity region

$$\frac{G}{G_{max}} = \left(\frac{G}{G_{max}}\right)_{x=x_p} + \left(\frac{d\dfrac{G}{G_{max}}}{dx}\right)_{x=x_p} x_\Delta$$

using Eq. 2 to determine the components of $d\ell$ and S in the $\bar{X}'$, $\bar{Y}'$, $\bar{Z}'$ coordinate system, discarding third and higher-order terms in the products of the small quantities y_Δ and x_Δ in the expressions

$$S_{\bar{X}} d\ell_{\bar{Z}} - S_{\bar{Z}} d\ell_{\bar{X}}$$

$$S^2 = S_X^2 + S_Y^2 + S_Z^2$$

and substituting into Eq. 15 yields the expressions for $(\Delta W_{\bar{Y}})_B / v_s$.

$$\frac{(\Delta W_{\bar{Y}})_B}{v_s} = \frac{1}{2} \int_{-\Delta y_n/2}^{\Delta y_n/2} (H_n + K_n y_\Delta)(C_1 y_\Delta + C_2 y_\Delta^2) \int_{-\Delta x/2}^{\Delta x/2} \frac{E + F x_\Delta}{(a_1 y_\Delta^2 + b_1 y_\Delta x_\Delta + c_1 x_\Delta^2)^{3/2}} \, dx_\Delta \, dy_\Delta \quad (26)$$

where

$$H_n = \left(\frac{dG_{max}}{dy}\right)_{y=y_n=y_p}$$

$$K_n = \left(\frac{d^2 G_{max}}{dy^2}\right)_{y=y_n=y_p}$$

$$C_1 = -f_{1p} \sin\beta_p - x_p f_{3p} \cos\beta_p$$

$$C_2 = f_{3p}(f_{1p} \sin\beta_p + x_p f_{3p} \cos\beta_p)[y_p(f_{7p} - f_{3p}) - (f_{8p} - f_{4p})]$$

$$E = \left(\frac{G}{G_{max}}\right)_{x=x_p}$$

$$F = \left(\frac{d\dfrac{G}{G_{max}}}{dx}\right)_{x=x_p}$$

$$a_1 = f_{1p}^2 + x_p^2 f_{3p}^2$$

$$b_1 = 2f_{1p}[y_p f_{5p} - f_{6p}) + 2x_p f_{3p}[y_p(f_{7p} - f_{3p}) - (f_{8p} - f_{4p})]$$

$$c_1 = (y_p f_{5p} - f_{6p})^2 + 1 + [y_p(f_{7p} - f_{3p}) - (f_{8p} - f_{4p})]^2$$

The integrations in Eq. 26 are straightforward but because they lead to lengthy expressions, they are not presented here. It suffices that Eq. 26 can be integrated analytically through the singularity to obtain the Cauchy principal value.

VELOCITY DUE TO FREE VORTICITY $(W_{\overline{\gamma}})_F$

The coordinates of a point on the helical sheets in the rectangular X', Y', Z' coordinate system were given as Eq. 1 and are repeated here.

$$X' = \alpha r \tan\beta$$

$$Y' = -r \sin(\psi_m + \alpha)$$

$$Z' = r \cos(\psi_m + \alpha) \qquad (1)$$

Assuming that the propeller is moderately loaded, the contraction of the wake may be neglected. Hence, each vortex element of the free vorticity sheets may be considered to lie on the helical sheet at a constant radius, as indicated in Fig. 8. Letting $d\ell$ be an infinitesimal

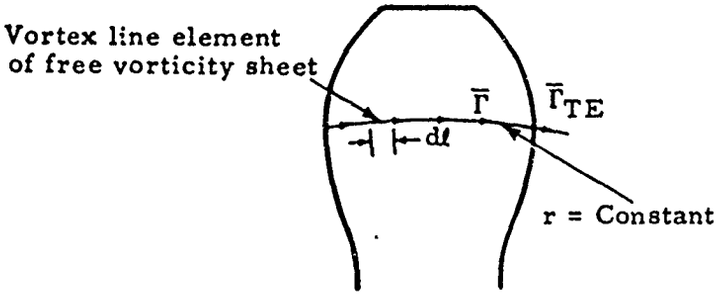

FIG. 8.

length of a vortex line element making up the free vorticity sheets, the components of $d\ell$ in the X', Y', Z' system are obtained from Eq. 1 as follows.

$$\frac{d\ell_X}{d\alpha} = \left.\frac{dX'}{d\alpha}\right|_{r=\text{Constant}}$$

$$\frac{d\ell_X}{d\alpha} = r \tan\beta$$

$$\frac{d\ell_Y}{d\alpha} = \left.\frac{dY'}{d\alpha}\right|_{r=\text{Constant}}$$

$$\frac{d\ell_Y}{d\alpha} = -r \cos(\psi_m + \alpha)$$

$$\frac{d\ell_Z}{d\alpha} = \left.\frac{dZ'}{d\alpha}\right|_{r=\text{Constant}}$$

$$\frac{d\ell_Z}{d\alpha} = -r \sin(\psi_m + \alpha)$$

The coordinates in the X', Y', Z' system of the point p on the blade $\psi_1 = 0$ where the normal component of velocity is desired is designated using the subscript p, as in the previous section.

$$X'_p = a_p r_p \tan\beta_p$$

$$Y'_p = -r_p \sin a_p$$

$$Z'_p = r_p \cos a_p \qquad (27)$$

The expression relating a_p to the position on the blade, developed in the preceding section, is

$$a_p = y_p f_{3p} - f_{4p}$$

The X', Y', Z' components of the distance, S, from an element of vorticity on one of the blades to the point p are obtained from Eq. 1 and 27.

$$S_X = X'_p - \alpha r \tan\beta$$

$$S_Y = Y'_p + r \sin(\psi_m + \alpha)$$

$$S_Z = Z'_p - r \cos(\psi_m + \alpha)$$

Introducing the nondimensional coordinates of Eq. 7, and letting $x \tan\beta = \lambda$, the components of $d\ell$ and S become

$$\frac{d\ell_X}{R d\alpha} = \lambda$$

$$\frac{d\ell_Y}{Rda} = -x \cos(\psi_m + a)$$

$$\frac{d\ell_Z}{Rda} = -x \sin(\psi_m + a)$$

$$\frac{S_X}{R} = X_p - a\lambda$$

$$\frac{S_Y}{R} = Y_p + x \sin(\psi_m + a)$$

$$\frac{S_Z}{R} = Z_p - x \cos(\psi_m + a) \qquad (28)$$

where

$$X_p = a_p(\lambda)_{x=x_p}$$

$$Y_p = -x_p \sin a_p$$

$$Z_p = x_p \cos a_p$$

Lifting-line solutions for free-running, unskewed, optimum or lightly loaded non-optimum propellers yield λ = Constant, i.e., independent of the spanwise station x. This is not true for moderately loaded, non-optimum, wake-adapted propellers, which are of interest here. To be able to handle this variation in λ, the blades are broken up into chordwise strips bounded by lines x = Constant, as illustrated in Fig. 9.

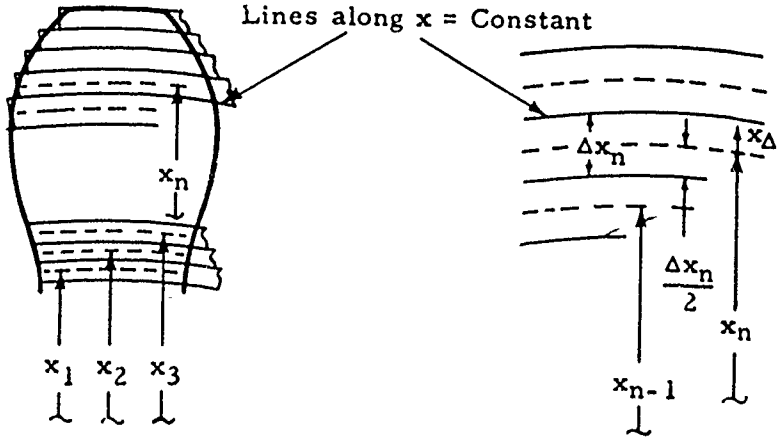

FIG. 9.

Due to the great simplification in the mathematical expressions which result, the location of points along a strip are described in terms of the angle α corresponding to the center of the strip. This causes the strips not to fit the blade shape exactly, as illustrated in Fig. 9 by the fact that the ends of the strips do not coincide with the leading edge. However, by using a fairly large number of strips, the blade shape can be represented quite accurately. For each strip there may be written

$$x = x_n + x_\Delta \tag{29}$$

The subscript n takes on values of 1, 2, 3, ..., i, where i is the number of strips. With the blade broken up into a fairly large number of strips, the variation in λ can be represented with sufficient accuracy by a linear approximation across each strip.

$$\lambda = (\lambda)_{x=x_n} + \left(\frac{d\lambda}{dx}\right)_{x=x_n} x_\Delta \tag{30}$$

Substituting Eq. 29 and 30 in Eq. 28, the expressions for the components of $d\ell$ and S become

$$\frac{d\ell_X}{R\,d\alpha} = (\lambda)_{x=x_n} + \left(\frac{d\lambda}{dx}\right)_{x=x_n} x_\Delta$$

$$\frac{d\ell_Y}{R\,d\alpha} = -x_n \cos(\psi_m + \alpha) - \cos(\psi_m + \alpha)x_\Delta$$

$$\frac{d\ell_Z}{R\,d\alpha} = -x_n \sin(\psi_m + \alpha) - \sin(\psi_m + \alpha)x_\Delta$$

$$\frac{S_X}{R} = X_p - \alpha(\lambda)_{x=x_n} - \alpha\left(\frac{d\lambda}{dx}\right)_{x=x_n} x_\Delta$$

$$\frac{S_Y}{R} = Y_p + x_n \sin(\psi_m + \alpha) + \sin(\psi_m + \alpha)x_\Delta$$

$$\frac{S_Z}{R} = Z_p - x_n \cos(\psi_m + \alpha) - \cos(\psi_m + \alpha)x_\Delta \tag{31}$$

The Biot-Savart law, Eq. 14, is used to compute the induced velocities from the free vorticity. Since only the normal component of velocity is desired, Eq. 15 gives the desired relationship. The strength, $\overline{\Gamma}$, of the vortex element as a function of the spanwise and chordwise

distribution of free vorticity is determined as follows. The value of $\bar{\Gamma}$ at the trailing edge of the blade, $\bar{\Gamma}_{TE}$ (Fig. 8), in terms of the bound circulation Γ is given by,

$$\bar{\Gamma}_{TE} = -\frac{d\Gamma}{dx}\,dx$$

A factor k is defined as the ratio of the strength $\bar{\Gamma}$ at any chordwise station to the strength at the trailing edge, $\bar{\Gamma}_{TE}$.

$$k = \frac{\bar{\Gamma}}{\bar{\Gamma}_{TE}}$$

Introducing once again the nondimensional bound circulation $G = \Gamma/\pi D v_s$ the expression for $\bar{\Gamma}$ is

$$\frac{\bar{\Gamma}}{\pi D v_s} = -k\frac{dG}{dx}\,dx \tag{32}$$

Considering an infinitesimal area on the blade bounded by lines y = Constant and x = Constant and utilizing the fact that the sum of the bound circulation and free vorticity entering the area must equal the sum of the bound circulation and free vorticity leaving the area, the expression, illustrated in Fig. 10, for k may be determined.

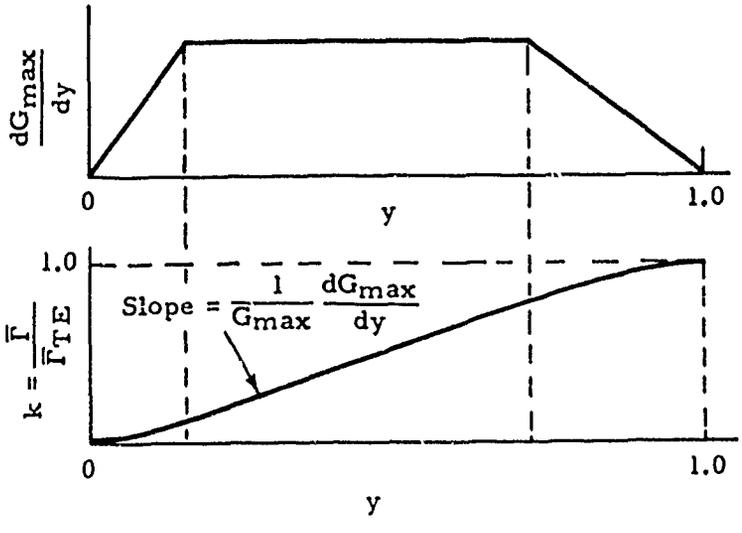

FIG. 10.

$$\text{For } 0 \leq y \leq 1 \qquad k = \frac{1}{G_{max}} \int_0^y \frac{dG_{max}}{dy}\, dy \qquad \text{For } y > 1 \qquad k = 1$$

This simple relationship between k and y, which is independent of the spanwise station, results from having chosen the elements of bound circulation along lines y = Constant. To obtain k as a function of a, the relation between a and y developed in the previous section is used.

$$a = y(f_3)_{x=x_n} - (f_4)_{x=x_n}$$

Restricting the spanwise distribution of bound circulation to one that lends itself to an accurate piecewise approximation by parabolic sections, as discussed previously, Eq. 32 may be written, for each chordwise strip,

$$\frac{\bar{\Gamma}}{\pi D v_s} = -k\left[\left(\frac{dG}{dx}\right)_{x=x_n} + \left(\frac{d^2G}{dx^2}\right)_{x=x_n} x_\Delta\right] dx_\Delta \tag{33}$$

Equation 2 allows the components of $d\ell$ and S in the $\bar{X}'$, $\bar{Y}'$, $\bar{Z}'$ coordinate system to be determined from their components in the X', Y', Z' system, given by Eq. 31. Substituting these $\bar{X}'$, $\bar{Y}'$, $\bar{Z}'$ components and Eq. 33 into Eq. 15, the expression for the normal component of induced velocity due to the free vorticity becomes

$$\frac{(W_{\bar{Y}})_F}{v_s} = -\frac{1}{2} \sum_{m=1}^{g} \sum_{n=1}^{i} \int_{a_{LE}}^{a_u} k \int_{-\Delta x_n/2}^{\Delta x_n/2} \frac{A_0 I_n + (A_0 J_n + A_1 I_n)x_\Delta + (A_1 J_n + A_2 I_n)x_\Delta^2 + A_2 J_n x_\Delta^3}{(a + bx_\Delta + cx_\Delta^2)^{3/2}}\, dx_\Delta da \tag{34}$$

where

$$I_n = \left(\frac{dG}{dx}\right)_{x=x_n}$$

$$J_n = \left(\frac{d^2G}{dx^2}\right)_{x=x_n}$$

$$a = 2Y_p x_n \sin(\psi_m + a) - 2Z_p x_n \cos(\psi_m + a) + (X_p - aM_n)^2 + Y_p^2 + Z_p^2 + x_n^2$$

$$b = 2Y_p \sin(\psi_m + a) - 2Z_p \cos(\psi_m + a) + 2x_n - 2aN_n(X_p - aM_n)$$

$$c = 1 - a^2 N_n^2$$

$$A_0 = -\{(X_p - aM_n)x_n \sin(\psi_m + a - a_p) - M_n[x_n \cos(\psi_m + a - a_p) + Y_p \sin a_p - Z_p \cos a_p]\}\sin\beta_p + x_n[Y_p \sin(\psi_m + a) - Z_p \cos(\psi_m + a) + x_n]\cos\beta_p$$

$$A_1 = -\{[(X_p - aM_n) - aN_n x_n]\sin(\psi_m + a - a_p) - (M_n + N_n x_n)\cos(\psi_m + a - a_p) - N_n(Y_p \sin a_p - Z_p \cos a_p)\}\sin\beta_p + [Y_p \sin(\psi_m + a) - Z_p \cos(\psi_m + a) + 2x_n]\cos\beta_p$$

$$A_2 = N_n[a \sin(\psi_m + a - a_p) + \cos(\psi_m + a - a_p)]\sin\beta_p + \cos\beta_p$$

and where

$$M_n = (\lambda)_{x=x_n}$$

$$N_n = \left(\frac{d\lambda}{dx}\right)_{x=x_n}$$

The integration with respect to x_Δ in Eq. 34 may be carried out analytically. The integration with respect to a must be carried out numerically. Performing the integration with respect to x_Δ, and since the numerical integration with respect to a cannot be carried through the singularity, Eq. 34 becomes

$$\frac{(W\bar{Y})F}{v_s} = -\frac{1}{2}\sum_{m=1}^{g}\sum_{n=1}^{i}\left(\int_{a_{LE}}^{a_p-\epsilon} kQda + \int_{a_p+\epsilon}^{a_u} kQda\right) + \frac{(\Delta W\bar{Y})F}{v_s} \qquad (35)$$

where

$$\epsilon = 0 \text{ for } m \neq 1 \quad \text{or} \quad x_n \neq x_p$$

$$\epsilon = \frac{\Delta a}{2} \text{ for } m = 1 \quad \text{and} \quad x_n = x_p$$

*For $|4ac - b^2| \geq 0.00001$

$$Q = \frac{A_2 J_n}{c}\left[\frac{x_\Delta^0}{(a + bx_\Delta + cx_\Delta^2)^{1/2}}\right]_{-\Delta x_n/2}^{\Delta x_n/2}$$

$$+ \frac{A_1 J_n + A_2\left(I_n - J_n \frac{3b}{2c}\right)}{c(4ac - b^2)}\left[\frac{(2b^2 - 4ac)x_\Delta + 2ab}{(a + bx_\Delta + cx_\Delta^2)^{1/2}}\right]_{-\Delta x_n/2}^{\Delta x_n/2}$$

$$+ \frac{A_1 J_n + A_2\left(I_n - J_n \frac{3b}{2c}\right)}{c^{3/2}}\left\{\ln\left[(a + bx_\Delta + cx_\Delta^2)^{1/2} + \sqrt{c}x_\Delta + \frac{b}{2\sqrt{c}}\right]\right\}_{-\Delta x_n/2}^{\Delta x_n/2}$$

$$- \frac{2\left(A_0 J_n + A_1 I_n - A_2 J_n \frac{2a}{c}\right)}{4ac - b^2}\left[\frac{bx_\Delta + 2a}{(a + bx_\Delta + cx_\Delta^2)^{1/2}}\right]_{-\Delta x_n/2}^{\Delta x_n/2}$$

$$+ \frac{2A_0 I_n}{4ac - b^2}\left[\frac{2cx_\Delta + b}{(a + bx_\Delta + cx_\Delta^2)^{1/2}}\right]_{-\Delta x_n/2}^{\Delta x_n/2}$$

*For $|4ac - b^2| < 0.00001$

$$Q = \frac{A_2 J_n}{c^2}\left(\sqrt{a} + \frac{b}{2\sqrt{a}}x_\Delta\right)_{-\Delta x_n/2}^{\Delta x_n/2}$$

$$+ \frac{A_1 J_n \frac{2\sqrt{a}}{b} + A_2\left(I_n \frac{2\sqrt{a}}{b} - J_n \frac{3\sqrt{a}}{c}\right)}{c}\left[\ln\left(\sqrt{a} + \frac{b}{2\sqrt{a}}x_\Delta\right)\right]_{-\Delta x_n/2}^{\Delta x_n/2}$$

*Under certain circumstances when $a = a_p$, $4ac - b^2 = 0$. The solution takes a different form at this point. Due to machine accuracy, the test is made on a small finite quantity rather than on zero.

$$-\frac{A_0 J_n + A_1\left(I_n - J_n\frac{4a}{b}\right) - A_2\left(I_n\frac{4a}{b} - J_n\frac{3a}{c}\right)}{c}\left[\frac{1}{\sqrt{a}+\frac{b}{2\sqrt{a}}x_\Delta}\right]_{-\Delta x_n/2}^{\Delta x_n/2}$$

$$-\left[A_0\left(I_n\frac{\sqrt{a}}{b} - J_n\frac{\sqrt{a}}{2c}\right) - A_1\left(I_n\frac{\sqrt{a}}{2c} - J_n\frac{a^{3/2}}{bc}\right) + A_2\left(I_n\frac{a^{3/2}}{bc} - J_n\frac{a^{3/2}}{2c^2}\right)\right]$$

$$\left[\frac{1}{\left(\sqrt{a}+\frac{b}{2\sqrt{a}}x_\Delta\right)^2}\right]_{-\Delta x_n/2}^{\Delta x_n/2}$$

and where $(\Delta W\bar{Y})_F$ is the contribution to $(W\bar{Y})_F$ from the small region surrounding the singularity. The determination of $(\Delta W\bar{Y})_F$ will follow shortly. The value of a at the leading edge, a_{LE}, follows from the work in the previous section.

$$a_{LE} = -(f_4)_{x=x_n}$$

The value of the upper limit of integration, a_u, is theoretically infinity; however, as is discussed subsequently, the integration may be truncated at a rather small value of a_u. Assuming that the integration is carried out q propeller diameters (measured axially) behind the point p where the velocity is desired, the expression for a_u is

$$a_u = \frac{2q + a_p(\lambda)_{x=x_p}}{(\lambda)_{x=x_n}}$$

This follows from the first of Eq. 1.

Since the lifting-surface solution starts from the lifting-line solution, the angularity of the flow due to the lifting-line solution has already been accounted for. Hence, only the difference between the normal component of velocity on the lifting surface and the normal component of velocity at the lifting line from the lifting-line solution is desired. It is of course understood that both these velocities are determined at the same radius. For free-running, optimum or lightly loaded non-optimum propellers where the helical sheets form a true helix, i.e., $\lambda = x\tan\beta$ = Constant, it is necessary in determining this difference to choose a value of q which assures only that the integrations are carried out to a point behind the trailing edge. This is true because for the true helix the integration from q diameters behind any point (at

a given radius) to infinity will be the same, so that upon taking the difference this contribution cancels out exactly. This fact has been taken advantage of by several investigators in calculating lifting-surface corrections for free-running, optimum, or lightly loaded non-optimum propellers. For all other propellers, such as the moderately loaded, non-optimum, wake-adapted propellers of interest here, the helical sheets do not form a true helix and this canceling effect does not occur. Luckily for these cases, the difference between the lifting-surface solution and the lifting-line solution is strongly dependent on q only for small values of q. Thus it is necessary to carry out the integration only a few propeller diameters behind the two points when determining this difference. A great saving in computer time results from this approach, since numerical integrations to great distances behind the propeller are not needed.

The normal component of velocity at the lifting line from a lifting-line solution where the integration is carried out q propeller diameters behind the lifting line is needed to determine the difference discussed above. This is determined from Eq. 35 by putting $\alpha_p = 0$, $k = 1$, and ignoring the integral from α_{LE} to $\alpha_p - \epsilon$. The expression for $(\Delta W \bar{Y})_F$ takes a different form for the lifting-line solution, as will be indicated later.

Figure 11 shows the small region surrounding the singularity. This region lies on the blade $\psi_1 = 0$ and has its center at the point $x_n = x_p$.

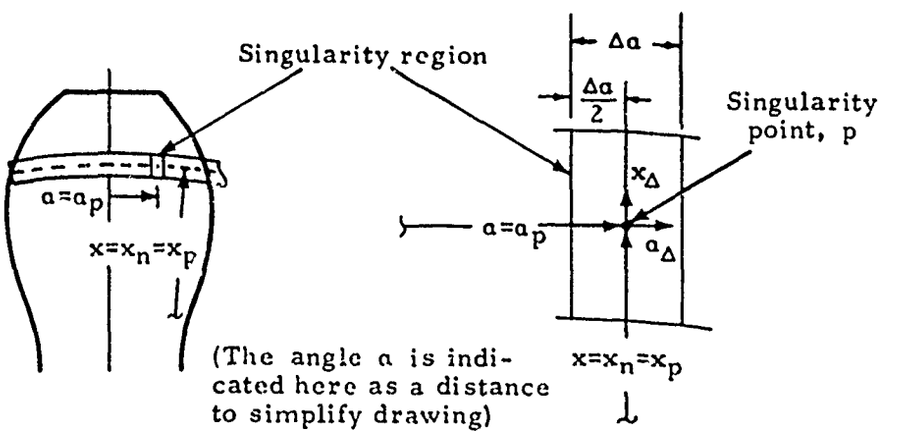

FIG. 11.

The location of points within this region is given by the nondimensional coordinate x_Δ and the angle α_Δ. Since x_Δ is nondimensionalized with respect to the propeller radius, it is very small compared to one. Also, α_Δ is restricted to be very small compared to one. The nondimensional coordinates in the X', Y', Z' system of points on the blade $\psi_1 = 0$ are, from Eq. 1 and 7

$$X = \alpha x \tan\beta = a\lambda$$

$$Y = -x \sin\alpha$$

$$Z = :: \cos\alpha \qquad (36)$$

In the region surrounding the singularity,

$$x = x_n + x_\Delta = x_p + x_\Delta, \qquad \alpha = \alpha_p + \alpha_\Delta$$

Substituting these expressions and Eq. 30 into Eq. 36, and making use of the trigonometric identities for the sin and cos of the sum of angles,

$$X = (a_p + a_\Delta)\left[(\lambda)_{x=x_p} + \left(\frac{d\lambda}{dx}\right)_{x=x_p} x_\Delta\right]$$

$$Y = -(x_p + x_\Delta)(\sin\alpha_p \cos\alpha_\Delta + \cos\alpha_p \sin\alpha_\Delta)$$

$$Z = (x_p + x_\Delta)(\cos\alpha_p \cos\alpha_\Delta - \sin\alpha_p \sin\alpha_\Delta) \qquad (37)$$

Since $(\alpha_\Delta)_{max} = \Delta\alpha/2$ is restricted to be very small compared to one (in radian measure),

$$\cos\alpha_\Delta \cong 1, \qquad \sin\alpha_\Delta \cong \alpha_\Delta$$

Putting these approximations in Eq. 37, there is obtained

$$X = a_p(\lambda)_{x=x_p} + a_p\left(\frac{d\lambda}{dx}\right)_{x=x_p} x_\Delta + \left(\frac{d\lambda}{dx}\right)_{x=x_p} x_\Delta a_\Delta + (\lambda)_{x=x_p} a_\Delta$$

$$Y = -x_p \sin\alpha_p - \sin\alpha_p x_\Delta - \cos\alpha_p x_\Delta a_\Delta - x_p \cos\alpha_p a_\Delta$$

$$Z = x_p \cos\alpha_p + \cos\alpha_p x_\Delta - \sin\alpha_p x_\Delta a_\Delta - x_p \sin\alpha_p a_\Delta \qquad (38)$$

Using Eq. 38 and the expressions on page 24 for $X_p Y_p Z_p$, the expressions for the components of $d\ell$ and S in the X', Y', Z' coordinate system are easily obtained.

$$\frac{d\ell_X}{da_\Delta} = \left.\frac{dX'}{da_\Delta}\right|_{x_\Delta=\text{Constant}} = R \left.\frac{dX}{da_\Delta}\right|_{x_\Delta=\text{Constant}}$$

$$\frac{d\ell_X}{R\,da_\Delta} = (\lambda)_{x=x_p} + \left(\frac{d\lambda}{dx}\right)_{x=x_p} x_\Delta$$

$$\frac{d\ell_Y}{da_\Delta} = \left.\frac{dY'}{da_\Delta}\right|_{x_\Delta=\text{Constant}} = R\left.\frac{dY}{da_\Delta}\right|_{x_\Delta=\text{Constant}}$$

$$\frac{d\ell_Y}{Rda_\Delta} = -x_p \cos a_p - \cos a_p x_\Delta$$

$$\frac{d\ell_Z}{da_\Delta} = \left.\frac{dZ'}{da_\Delta}\right|_{x_\Delta=\text{Constant}} = R\left.\frac{dZ}{da_\Delta}\right|_{x_\Delta=\text{Constant}}$$

$$\frac{d\ell_Z}{Rda_\Delta} = -x_p \sin a_p - \sin a_p x_\Delta$$

$$S_X = X'_p - X' = R(X_p - X)$$

$$\frac{S_X}{R} = -a_p\left(\frac{d\lambda}{dx}\right)_{x=x_p} x_\Delta - \left(\frac{d\lambda}{dx}\right)_{x=x_p} x_\Delta a_\Delta - (\lambda)_{x=x_p} a_\Delta$$

$$S_Y = Y'_p - Y' = R(Y_p - Y)$$

$$\frac{S_Y}{R} = \sin a_p x_\Delta + \cos a_p x_\Delta a_\Delta + x_p \cos a_p a_\Delta$$

$$S_Z = Z'_p - Z' = R(Z_p - Z)$$

$$\frac{S_Z}{R} = -\cos a_p x_\Delta + \sin a_p x_\Delta a_\Delta + x_p \sin a_p a_\Delta$$

Making a linear approximation in Eq. 33 to k across the singularity region,

$$k = (k)_{a=a_p} + \left(\frac{dk}{da}\right)_{a=a_p} a_\Delta$$

using Eq. 2 to determine the components of $d\ell$ and S in the $\bar{X}'$, $\bar{Y}'$, $\bar{Z}'$ coordinate system, discarding third and higher-order terms in the products of the small quantities x_Δ and a_Δ in the expression

$$S^2 = S_X^2 + S_Y^2 + S_Z^2$$

and substituting into Eq. 15 yields the expression for $(\Delta W_{\bar{Y}})_F$.

$$\frac{(\Delta W_{\bar{Y}})_F}{v_s} = -\frac{1}{2}\int_{-\Delta x_n/2}^{\Delta x_n/2} (I_n + J_n x_\Delta)(C_1 x_\Delta + C_2 x_\Delta^2) \int_{-\Delta a/2}^{\Delta a/2} \frac{k_0 + k_1 a_\Delta}{(a_1 x_\Delta^2 + b_1 x_\Delta a_\Delta + c_1 a_\Delta^2)^{3/2}}\, da_\Delta dx_\Delta \quad (39)$$

where

$$I_n = \left(\frac{dG}{dx}\right)_{x=x_n=x_p}$$

$$J_n = \left(\frac{d^2G}{dx^2}\right)_{x=x_n=x_p}$$

$$k_0 = (k)_{a=a_p}$$

$$k_1 = \left(\frac{dk}{da}\right)_{a=a_p}$$

$$C_1 = M_n \sin\beta_p + x_p \cos\beta_p$$

$$C_2 = N_n \sin\beta_p + \cos\beta_p$$

$$a_1 = 1 - a_p^2 N_n^2$$

$$b_1 = 2a_p M_n N_n$$

$$c_1 = M_n^2 + x_p^2$$

and where

$$M_n = (\lambda)_{x=x_n=x_p}$$

$$N_n = \left(\frac{d\lambda}{dx}\right)_{x=x_n=x_p}$$

For the lifting-line solution, where the point p is at the front edge of the helical sheet and there is no variation in the strength of the sheet with respect to α, the lower limit of integration with respect to α_Δ should be zero instead of $-\Delta\alpha/2$, and the values of k_0 and k_1 should be one and zero, respectively. The integrations in Eq. 39 can be carried out analytically through the singularity to obtain the Cauchy principal value. These integrations lead to lengthy expressions that are not presented here.

VELOCITY DUE TO BLADE THICKNESS $(W\bar{Y})_T$

In calculating the effect of blade thickness, the blades are broken up into spanwise strips like those used in the section on bound circulation. Hence, many expressions take the same form and are taken directly from that section.

The components of the distance, S, from a point on one of the blades to the point p where the velocity is desired are given by Eq. 13 and are repeated here.

$$\frac{S_X}{R} = X_p - y_n f_1 + f_2 - f_1 y_\Delta$$

$$\frac{S_Y}{R} = Y_p + x \sin(\psi_m + y_n f_3 - f_4) + x f_3 \cos(\psi_m + y_n f_3 - f_4) y_\Delta$$

$$\frac{S_Z}{R} = Z_p - x \cos(\psi_m + y_n f_3 - f_4) + x f_3 \sin(\psi_m + y_n f_3 - f_4) y_\Delta \qquad (13)$$

Since the velocity at point p caused by a source (representing the blade thickness) on one of the blades is desired, the source potential may be written

$$\phi = \frac{\eta}{4\pi}\frac{1}{S} = \frac{\eta}{4\pi}\frac{1}{\sqrt{S_X^2 + S_Y^2 + S_Z^2}}$$

where η is the source strength.

The components of the induced velocity at point p in the X', Y', Z' directions from the source are given by

$$-\frac{\partial\phi}{\partial S_X} = W_X = \frac{\eta}{4\pi}\frac{S_X}{(S_X^2 + S_Y^2 + S_Z^2)^{3/2}}$$

$$-\frac{\partial\phi}{\partial S_Y} = W_Y = \frac{\eta}{4\pi}\frac{S_Y}{(S_X^2 + S_Y^2 + S_Z^2)^{3/2}}$$

$$-\frac{\partial\phi}{\partial S_Z} W_Z = \frac{\eta}{4\pi} \frac{S_Z}{(S_X^2 + S_Y^2 + S_Z^2)^{3/2}}$$

Equation 2 allows the normal component of velocity, $W_{\bar{Y}}$, to be determined from the preceding result. The normal component of velocity at point p due to a source of infinitesimal strength on one of the blades is then written

$$dW_{\bar{Y}} = \frac{d\eta}{4\pi} \frac{S_X \cos\beta_p + S_Y \cos\alpha_p \sin\beta_p + S_Z \sin\alpha_p \sin\beta_p}{(S_X^2 + S_Y^2 + S_Z^2)^{3/2}} \qquad (40)$$

The infinitesimal source strength can be written as a product of a surface source density on the helical sheet, μ, and an infinitesimal area, dA, of the sheet.

$$d\eta = \mu dA \qquad (41)$$

The source density can be related to the blade-section thickness distribution as is done in slender-airfoil theory and illustrated in Fig. 12.

$$\mu = 2V \frac{dz}{dy} * \qquad (42)$$

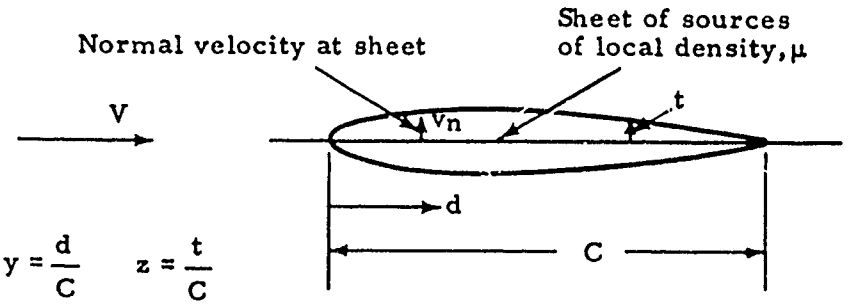

$$\frac{v_n}{V} \cong \frac{dz}{dy} \qquad v_n = \frac{\mu}{2}$$

$$\therefore \quad \mu \cong 2V \frac{dz}{dy}$$

FIG. 12.

*Since dz/dy goes to infinity as $y \to 0$ for essentially all thickness forms, the nose shape is modified slightly to retain a finite dz/dy at y = 0.

The relative velocity V of the blade section and the fluid is given approximately for a propeller by

$$V = \sqrt{(v + W_a)^2 + (\omega r - W_t)^2}$$

where v is the local axial inflow velocity to the propeller, ω is the angular velocity of the propeller, and W_a and W_t are the axial and tangential components of induced velocity from the lifting-line solution. Assuming that the thickness distribution function, $z = f(y)$, is the same at all spanwise stations except for a multiplier that is a function of x only,[1] it is necessary to specify it at only one station. Hence,

$$\frac{dz}{dy} = \left(\frac{dz}{dy}\right)_{Ref} r_R \tag{43}$$

where r_R is the ratio of the percent thickness of the blade section at any spanwise station to the percent thickness at the reference station. The expression for the infinitesimal area, dA, of the helical sheets in terms of the nondimensional coordinates y and x can be determined by the use of Eq. 4, 5, 7, and 10 and relationships involving direction cosines. The expression is

$$dA = RC\sqrt{\{(yf_5 - f_6)\cos\beta + [f_8 - f_4 - y(f_7 - f_3)]\sin\beta\}^2 + 1}\, dy\, dx$$

Since the variation in y across a strip is not large, a fairly accurate approximate expression for dA may be obtained by setting y equal to the value at the center of the strip, y_n.

$$dA \cong RCF_n dy\, dx \tag{44}$$

where

$$F_n = \sqrt{\{(y_n f_5 - f_6)\cos\beta + f_8 - f_4 - y_n(f_7 - f_3)]\sin\beta\}^2 + 1}$$

Substituting Eq. 41, 42, 43, and 44 into Eq. 40, the normal component of velocity at point p due to the thickness effect of an infinitesimal area on one of the blades becomes

---

[1] This type of relation holds approximately for any of the NACA basic thickness-form groups. For example, the $z = f(Y)$ for the NACA 65-008 form can be obtained approximately from that for the NACA 65-010 by multiplying by 8/10.

$$\frac{dW_{\bar{Y}}}{v_s} = \frac{1}{\pi} f_0 F_n \frac{\left(\frac{dz}{dy}\right)_{Ref}\left(\frac{S_X}{R}\cos\beta_p + \frac{S_Y}{R}\cos\alpha_p \sin\beta_p + \frac{S_Z}{R}\sin\alpha_p \sin\beta_p\right)}{\left(\frac{S_X^2}{R^2} + \frac{S_Y^2}{R^2} + \frac{S_Z^2}{R^2}\right)^{3/2}} dy\,dx \quad (45)$$

where

$$f_0 = f(x) = \frac{V}{v_s}\frac{C}{D} r_R$$

Approximating the thickness distribution function across each strip by a parabola,

$$\left(\frac{dz}{dy}\right)_{Ref} = \left(\frac{dz}{dy}\right)_{y=y_n} + \left(\frac{d^2z}{dy^2}\right)_{y=y_n} y_\Delta \quad (46)$$

Substituting Eq. 46 into Eq. 45, and indicating the integration over the blades, the expression for the normal component of induced velocity due to blade thickness becomes

$$\frac{(W_{\bar{Y}})_T}{v_s} = \frac{1}{\pi}\sum_{m=1}^{g}\sum_{n=1}^{s}\int_{x_h}^{1} f_0 F_n \int_{-\Delta y_n/2}^{\Delta y_n/2} \frac{A_0 S_n + (A_0 T_n + A_1 S_n) y_\Delta + A_1 T_n y_\Delta^2}{(a + b y_\Delta + c y_\Delta^2)^{3/2}} dy_\Delta\,dx \quad (47)$$

where

$$S_n = \left(\frac{dz}{dy}\right)_{y=y_n}$$

$$T_n = \left(\frac{d^2z}{dy^2}\right)_{y=y_n}$$

$$A_0 = (X_p - y_n f_1 + f_2)\cos\beta_p + [Y_p \cos\alpha_p + Z_p \sin\alpha_p + x \sin(\psi_m + y_n f_3 - f_4 - \alpha_p)]\sin\beta_p$$

$$A_1 = -f_1 \cos\beta_p + x f_3 \cos(\psi_m + y_n f_3 - f_4 - \alpha_p)\sin\beta_p$$

$$a = 2Y_p x \sin(\psi_m + y_n f_3 - f_4) - 2Z_p x \cos(\psi_m + y_n f_3 - f_4) + (X_p - y_n f_1 + f_2)^2 + Y_p^2 + Z_p^2 + x^2$$

$$b = 2Y_p x f_3 \cos(\psi_m + y_n f_3 - f_4) + 2Z_p x f_3 \sin(\psi_m + y_n f_3 - f_4) - 2f_1(X_p - y_n f_1 + f_2)$$

$$c = x^2 f_3^2 + f_1^2$$

The integration with respect to y_Δ in Eq. 47 can be carried out analytically. The integration with respect to x must be carried out numerically. Carrying out the integration with respect to y_Δ and since the numerical integration with respect to x cannot be carried through the singularity, Eq. 47 becomes

$$\frac{(W\overline{Y})_T}{v_s} = \frac{1}{\pi} \sum_{m=1}^{g} \sum_{n=1}^{s} \left(\int_{x_h}^{x_p - \epsilon} f_0 F_n Q dx + \int_{x_p + \epsilon}^{1} f_0 F_n Q dx \right) + \frac{(\Delta W\overline{Y})_T}{v_s}$$

where

$$\epsilon = 0 \text{ for } m \neq 1 \quad \text{or} \quad y_n \neq y_p$$

$$\epsilon = \frac{\Delta x}{2} \text{ for } m = 1 \quad \text{and} \quad y_n = y_p$$

*For $|4ac - b^2| > 0.00001$

$$Q = \frac{2A_0 S_n}{4ac - b^2} \left[\frac{2cy_\Delta + b}{(a + by_\Delta + cy_\Delta^2)^{1/2}} \right]_{-\Delta y_n/2}^{\Delta y_n/2} - \frac{2(A_0 T_n + A_1 S_n)}{4ac - b^2} \left[\frac{by_\Delta + 2a}{(a + by_\Delta + cy_\Delta^2)^{1/2}} \right]_{-\Delta y_n/2}^{\Delta y_n/2} + \frac{A_1 T_n}{c(4ac - b^2)} \left[\frac{(2b^2 - 4ac)y_\Delta + 2ab}{(a + by_\Delta + cy_\Delta^2)^{1/2}} \right]_{-\Delta y_n/2}^{\Delta y_n/2} + \frac{A_1 T_n}{c^{3/2}} \left\{ \ln \left[(a + by_\Delta + cy_\Delta^2)^{1/2} + \sqrt{c}y + \frac{b}{2\sqrt{c}} \right] \right\}_{-\Delta y_n/2}^{\Delta y_n/2}$$

*Under certain circumstances when $x = x_p$, $4ac - b^2 = 0$ (exactly or within the accuracy of the computer). The solution takes a different form at this point. Due to machine accuracy, the test is made on a small finite quantity rather than on zero.

*For $|4ac - b^2| \leq 0.00001$

$$Q = -\left[A_0\left(S_n\frac{\sqrt{a}}{b} - T_n\frac{\sqrt{a}}{2c}\right) - A_1\left(S_n\frac{\sqrt{a}}{2c} - T_n\frac{a^{3/2}}{bc}\right)\right]\left[\frac{1}{\left(\sqrt{a} + \frac{b}{2\sqrt{a}}y_\Delta\right)^2}\right]_{-\Delta y_n/2}^{\Delta y_n/2}$$

$$- \frac{A_0T_n + A_1\left(S_n - T_n\frac{4a}{b}\right)}{c}\left[\frac{1}{\sqrt{a} + \frac{b}{2\sqrt{a}}y_\Delta}\right]_{-\Delta y_n/2}^{\Delta y_n/2}$$

$$+ A_1T_n\frac{2\sqrt{a}}{bc}\left[\ln\left(\sqrt{a} + \frac{b}{2\sqrt{a}}y_\Delta\right)\right]_{-\Delta y_n/2}^{\Delta y_n/2}$$

and where $(\Delta W\bar{Y})_T$ is the contribution to $(W\bar{Y})_T$ from the small region surrounding the singularity. The determination of $(\Delta W\bar{Y})_T$ follows.

The small region surrounding the singularity is similar to that in the section on bound circulation and is shown in Fig. 7. The expressions for the X', Y', Z' components of S inside the singularity region are given by Eq. 25 and repeated here.

$$\frac{S_X}{R} = -f_{1p}y_\Delta - f_{5p}y_\Delta x_\Delta - (y_pf_{5p} - f_{6p})x_\Delta$$

$$\frac{S_Y}{R} = x_pf_{3p}\cos\alpha_p y_\Delta + f_{3p}\{\cos\alpha_p - \sin\alpha_p[(y_p + y_\Delta)(f_{7p} - f_{3p}) - (f_{8p} - f_{4p})]\}y_\Delta x_\Delta$$
$$+ \{\sin\alpha_p + \cos\alpha_p[(y_p + y_\Delta)(f_{7p} - f_{3p}) - (f_{8p} - f_{4p})]\}x_\Delta$$

$$\frac{S_Z}{R} = x_pf_{3p}\sin\alpha_p y_\Delta + f_{3p}\{\sin\alpha_p + \cos\alpha_p[(y_p + y_\Delta)(f_{7p} - f_{3p}) - f_{8p} - f_{4p})]\}y_\Delta x_\Delta$$
$$- \{\cos\alpha_p - \sin\alpha_p[(y_p + y_\Delta)(f_{7p} - f_{3p}) - (f_{8p} - f_{4p})]\}x_\Delta \quad (25)$$

Making a linear approximation of f_0 across the region,

$$f_0 = (f_0)_{x=x_p} + \left(\frac{df_0}{dx}\right)_{x=x_p} x_\Delta$$

using the value of F_n at the center of the region,

$$F_n = (F_n)_{\substack{x=x_p \\ y_n=y_p}} = F_p$$

discarding third and higher-order terms in the products of the small quantities y_Δ and x_Δ in the expressions

$$\left(\frac{dz}{dy}\right)_{Ref} (S_X \cos\beta_p + S_Y \cos\alpha_p \sin\beta_p + S_Z \sin\alpha_p \sin\beta_p)$$

$$S^2 = S_X^2 + S_Y^2 + S_Z^2$$

substituting into Eq. 45 and indicating the integration over the region, the expression for $(\Delta W_{\bar{Y}})_T$ is

$$\frac{(\Delta W_{\bar{Y}})_T}{v_s} = \frac{1}{\pi} F_p \int_{-\Delta x/2}^{\Delta x/2} (A + Bx_\Delta) \int_{-\Delta y_n/2}^{\Delta y_n/2} \frac{C_0 x_\Delta + C_1 x_\Delta y_\Delta}{(a_1 x_\Delta^2 + b_1 x_\Delta y_\Delta + c_1 y_\Delta^2)^{3/2}} dy_\Delta dx_\Delta \quad (48)$$

where

$$F_p = \sqrt{\{(y_p f_{5p} - f_{6p}) \cos\beta_p + [f_{8p} - f_{4p} - y_p(f_{7p} - f_{3p})] \sin\beta_p\}^2 + 1}$$

$$A = (f_0)_{x=x_p}$$

$$B = \left(\frac{df_0}{dx}\right)_{x=x_p}$$

$$C_0 = S_n\{[y_p(f_{7p} - f_{3p}) - (f_{8p} - f_{4p})] \sin\beta_p - (y_p f_{5p} - f_{6p}) \cos\beta_p\}$$

$$C_1 = T_n\{[y_p(f_{7p} - f_{3p}) - (f_{8p} - f_{4p})] \sin\beta_p - (y_p f_{5p} - f_{6p}) \cos\beta_p\} + S_n(f_{7p} \sin\beta_p - f_{5p} \cos\beta_p)$$

$$S_n = \left(\frac{dz}{dy}\right)_{y=y_n=y_p}$$

$$T_n = \left(\frac{d^2z}{dy^2}\right)_{y=y_n=y_p}$$

$$a_1 = (y_p f_{5p} - f_{6p})^2 + 1 + [y_p(f_{7p} - f_{3p}) - (f_{8p} - f_{4p})]^2$$

$$b_1 = 2f_{1p}(y_p f_{5p} - f_{6p}) + 2x_p f_{3p}[y_p(f_{7p} - f_{3p}) - (f_{8p} - f_{4p})]$$

$$c_1 = f_{1p}^2 + x_p^2 f_{3p}^2$$

The integration in Eq. 48 can be carried out analytically through the singularity to determine the Cauchy principal value. Due to the lengthy expression that results, this operation is not shown here.

DETERMINATION OF CAMBER LINES FROM NORMAL COMPONENT OF INDUCED VELOCITY

The total normal component of induced velocity desired for computing the camber lines is

$$W\bar{Y} = (W\bar{Y})_B + (W\bar{Y})_F - (W\bar{Y})_{FLL} + (W\bar{Y})_T$$

where $(W\bar{Y})_{FLL}$ is the normal component of induced velocity at the lifting line from the lifting-line solution. This component must be subtracted since the angularity of the flow due to the lifting-line solution has already been accounted for. This point was discussed in detail in the section on free vorticity. The nomenclature used in describing the camber lines is given in Fig. 13.

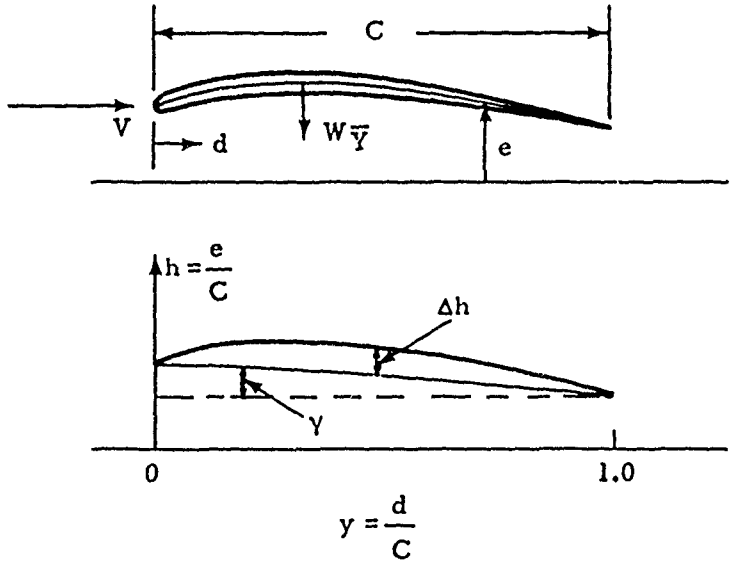

FIG. 13.

The camber lines are approximated by a power series of j + 1 terms.

$$h = a_0 + a_1 y + a_2 y^2 + a_3 y^3 + \cdots + a_j y^j$$

The slope of the camber line is related to the normal component of induced velocity $\overline{v}$

$$\frac{dh}{dy} = -\frac{W\overline{v}}{V}$$

Hence,

$$-\frac{W\overline{v}}{V} = a_1 + 2a_2 y + 3a_3 y^2 + \cdots + ja_j y^{j-1}$$

If $W\overline{v}$ is determined at j values of y across the blade, there result j linear equations in the j unknowns, a_i. Upon solving for the a_i, the camber offset, Δh, and the variation of the pitch angle from the lifting line value, γ, are determined from

$$\gamma = -\sum_{i=1}^{j} a_i$$

$$\Delta h = (y - 1)a_0 + (y - 1)a_1 + (y^2 - 1)a_2 + \cdots + (y^j - 1)a_j \qquad (49)$$

COMPUTER PROGRAMS

The foregoing equations for the solution of the induced velocities and the camber lines were programmed on an IBM 7090 computer. To facilitate program checkout, four separate programs were written: (1) solution of induced velocities due to bound circulation, (2) solution of induced velocities due to free vorticity, (3) solution of induced velocities due to blade thickness, and (4) solution of camber lines and angles of attack from induced velocities. The induction factor lifting-line solution of Lerbs (Ref. 2) was also programmed on the 7090 computer because it serves as the starting point of the lifting-surface solution. These five programs were thoroughly checked out against hand calculations and special cases for which exact solutions can be obtained. Some of the results and some typical design calculations for a wake-adapted propeller will be given in a future report on numerical results from the lifting-surface theory.

Simpson's rule was used in these programs when numerical integrations were needed. Although there are methods superior to Simpson's rule, it appeared more advantageous to gain accuracy by using more points in the numerical integration than to use a more complicated integration technique.

Examination of the foregoing mathematical developments shows that first and second derivatives of various functions are needed as inputs to the solution. Normally, these functions are known only as a table of

discrete values and determination of meaningful third or higher derivatives is very difficult. Consequently, the approach taken in the preceding mathematical developments was adopted, e.g., low-order approximations (involving at most second derivatives) were used across the strips and accuracy obtained by using many strips. The needed first and second derivatives could then be determined through a 7090 computer program existing at NOTS that allows a sliding polynomial fit by least squares to the discrete input data and outputs first and second derivatives.

RESTRICTION ON BLADE SHAPE

Blade shapes having rounded tips, as illustrated in Fig. 14, cannot be handled by this method because of the behavior of certain functions that appear in the numerical integrations.

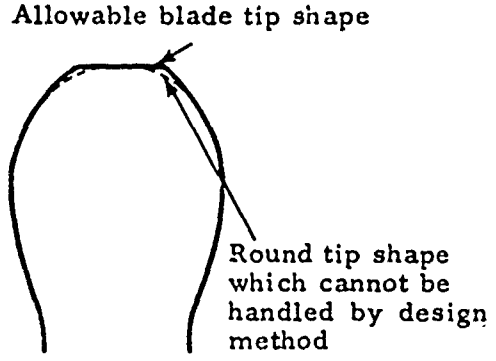

FIG. 14.

For rounded tips,

$$\left.\begin{aligned} f_5 &= \frac{d[2(C/D)\sin\beta]}{dx} \longrightarrow -\infty \\ f_6 &= \frac{d[2(L/D)\sin\beta]}{dx} \longrightarrow -\infty \\ f_7 &= \frac{d[2(C/D)\cos\beta]}{dx} \longrightarrow -\infty \\ f_8 &= \frac{d[2(L/D)\cos\beta]}{dx} \longrightarrow -\infty \end{aligned}\right\} \text{as } x \to 1$$

Also, the approximations of Eq. 22 can be made valid only if f_7 and f_8 do not become excessively large. Hence, this method is restricted to blade shapes that have a finite chord at the tip, as shown in Fig. 14. Since such a modification to the more usual rounded tip can result in at most a very small loss in propeller efficiency, no significant loss in the method's usefulness is caused by this blade-shape restriction.

DISCUSSION

The approach taken in the preceding work has been to obtain a satisfactory engineering solution to a difficult problem rather than to attempt an elegant development from a mathematical point of view. Therefore, this method must be used with a certain amount of engineering judgment in such things as the number and width of the strips into which the blades are divided and the size of the singularity region. The check solutions and design calculations that have been run to date provided sufficient knowledge for these judgments to be made now on a rational basis. A further discussion of this point, along with typical values, will be given in a future report presenting numerical results from the lifting-surface theory.

Verification of an interesting point has occurred in the calculations that have been run. For unskewed, free-running, optimum, or lightly loaded non-optimum ($\lambda = x \tan \beta$ = Constant) propellers having symmetrical blade shape, symmetrical chordwise loading, and negligible thickness, the pitch given by the lifting-surface solution is identical to that from the lifting-line solution (γ in Eq. 49 equals zero for all spanwise stations). This point has been referred to by several investigators. Hence, the pitch correction for such propellers arises solely from blade thickness.

CONCLUSIONS AND FUTURE WORK

The lifting-surface design method, with the aid of a high-speed computer, allows single-rotating, wake-adapted propellers of nearly arbitrary shape and loading to be designed without the need for the many assumptions and approximations involved in the methods that can be carried out with a hand calculator. Since the mathematical model accounts for nearly all parts of the physical propeller system in a fairly exact manner, there is reason to believe that propellers designed by this lifting-surface method will perform to specification. A definite conclusion cannot be made, of course, until propellers are designed and tested.

In torpedo design, counterrotating propellers are usually employed to obtain a torque balance. In order to apply the lifting-surface method, a lifting-line solution is under development for counterrotating propellers that will serve as the starting point for application of the lifting-surface solution to each propeller. The effect of each propeller on itself is

determined by a slightly modified version of Lerbs' induction-factor method that allows the effect of the interference velocities (those induced at one propeller by the other) to be accounted for in the relative flow at the lifting line and also allows application to propellers having a finite circulation at the hub.

The mean axial-induced velocities at one propeller induced by the other are obtained by replacing the finitely bladed propeller with an infinitely bladed propeller having the same radial thrust distribution. The mean tangential-induced velocities at the rear propeller caused by the front propeller are determined from Stokes' theorem. Continuity effects due to hub taper are accounted for in an approximate manner.

The one possibly important factor in propeller design, which to date has not been thoroughly investigated, is the effect of the hub boundary condition. Work has been done on optimum propellers where the hub boundary condition was satisfied in the ultimate wake; however, it has not been shown that this bears any relation to satisfying the boundary condition in the vicinity of the propeller. The possibility of satisfying the hub boundary condition in the vicinity of the propeller by using a surface source density on the hub is being considered. A method similar to that used by Smith and Hess (Ref. 12) would be used. Until the hub boundary condition is examined in some such fairly rigorous fashion, there will always remain a doubt as to the adequacy of even a lifting-surface design method.

Negative Numbers of Illustrations: None

REFERENCES

1. Eckhardt, M.K., and W.B.Morgan. "A Propeller Design Method," SOC NAVAL ARCH MARINE ENGR, TRANS, Vol.63, 1955.
2. Lerbs, H.W. "Moderately Loaded Propellers With a Finite Number of Blades and an Arbitrary Distribution of Circulation," SOC NAVAL ARCH MARINE ENGR, TRANS, Vol.60, 1952.
3. Aerodynamische Versuchsanstalt. On the Theory of Screws With Wide Blades, by H.Ludwieg and I.Ginzel. Goettingen, Germany, Aerodynamische Versuchsandstalt, 1944. (Rep.44/A/08.)
4. Admiralty Research Laboratory. Influence of Blade Shape and of Circulation Distribution on the Camber Correction Factor, by I. Ginzel. Teddington, England, ARL, August 1951. (R.2/G/HY/7/1.)
5. David Taylor Model Basin. Propeller Pitch Correction Arising From Lifting Surface Effect, by H.W.Lerbs. Washington, DTMB, 1955. (Report No.942.)
6. Pien, Pao C. "The Calculation of Marine Propellers Based on Lifting Surface Theory," J SHIP RES, Vol.5, No.2(September 1961).
7. Massachusetts Institute of Technology, Department of Naval Architecture and Marine Engineering. The Solution of Propeller Lifting Surface Problems by Vortex Lattice Methods, by J.E. Kerwin. Cambridge, Mass., MIT, June 1961.
8. Sparenberg, J.A. "Application of Lifting Surface Theory to Ship Screws," INTERN SHIPBLDG PROG, Vol.7, No.67 (March 1960).
9. Van Manen, J.D., and A.R. Bakker. "Numerical Results of Sparenberg's Lifting Surface Theory for Ship Screws," Fourth Symposium on Naval Hydrodynamics, PROC, Washington, August 1962.
10. Cox, G.G. "Corrections to the Camber of Constant Pitch Propellers," ROY INST NAVAL ARCH, TRANS, 1961.
11. Nishiyama, T. "Lifting Surface Theory of the Widely Bladed Marine Propellers," and Y. Nakajima, "Theory of the Wide-Bladed Propellers and Its Application," ZESEN KIOKAI J (Society of Naval Architects of Japan), Vol.109, 1961.
12. Douglas Aircraft Co., Aircraft Division. Calculation of the Non-lifting Potential Flow About Arbitrary Three-Dimensional Bodies, by J. L. Hess and A.M.O. Smith. Long Beach, Calif., Douglas, 15 March 1962. (Report No.E.S.40622.)

INITIAL DISTRIBUTION

6 Chief, Bureau of Naval Weapons
  DLI-31 (2)
  RAAD (1)
  RAAD-222 (1)
  RRRE (1)
  RUTO-32 (1)
9 Chief, Bureau of Ships
  Code 106 (1)
  Code 310 (1)
  Code 312 (1)
  Code 335 (1)
  Code 420 (1)
  Code 421 (1)
  Code 440 (1)
  Code 442 (1)
  Code 449 (1)
1 Chief, Bureau of Yards and Docks (Code D-400)
6 Chief of Naval Research
  Code 438 (3)
  Code 461 (1)
  Code 463 (1)
  Code 466 (1)
2 David W. Taylor Model Basin
  Code 526 (1)
  Code 526A (1)
1 Naval Research Laboratory (Code 2027)
2 Naval Weapons Services Office
1 Office of Naval Research Branch Office, Boston
1 Office of Naval Research Branch Office, London
1 Office of Naval Research Branch Office, New York
1 Office of Naval Research Branch Office, Pasadena
1 Office of Naval Research Branch Office, San Francisco
2 Army Transportation Research and Development Command, Fort Eustis (Marine Transport Division)
1 Aeonautical Systems Division, Wright-Patterson Air Force Base (Dynamics Branch, W. Mykytow)
1 Air Force Office of Scientific Research (Mechanics Branch)
10 Defense Documentation Center (TISIA-1)
1 National Aeronautics & Space Administration (Director of Research)
1 National Bureau of Standards (Fluid Mechanics Division, Dr. G. B. Schubauer)
1 National Science Foundation (Director Engineering Sciences Division)

ABSTRACT CARD

U. S. Naval Ordnance Test Station
A Lifting-Surface Propeller Design Method for High-Speed Computers, by D. M. Nelson. China Lake, Calif., NOTS, January 1964. 48 pp. (NAVWEPS Report 8442, NOTS TP 3399), UNCLASSIFIED.

ABSTRACT. A propeller design method that treats the blades as lifting surfaces has been developed and programmed on an IBM 7090 computer. The singularity distributions representing the bound

(Over)
1 card, 4 copies

U. S. Naval Ordnance Test Station
A Lifting-Surface Propeller Design Method for High-Speed Computers, by D. M. Nelson. China Lake, Calif., NOTS, January 1964. 48 pp. (NAVWEPS Report 8442, NOTS TP 3399), UNCLASSIFIED.

ABSTRACT. A propeller design method that treats the blades as lifting surfaces has been developed and programmed on an IBM 7090 computer. The singularity distributions representing the bound

(Over)
1 card, 4 copies

U. S. Naval Ordnance Test Station
A Lifting-Surface Propeller Design Method for High-Speed Computers, by D. M. Nelson. China Lake, Calif., NOTS, January 1964. 48 pp. (NAVWEPS Report 8442, NOTS TP 3399), UNCLASSIFIED.

ABSTRACT. A propeller design method that treats the blades as lifting surfaces has been developed and programmed on an IBM 7090 computer. The singularity distributions representing the bound

(Over)
1 card, 4 copies

U. S. Naval Ordnance Test Station
A Lifting-Surface Propeller Design Method for High-Speed Computers, by D. M. Nelson. China Lake, Calif., NOTS, January 1964. 48 pp. (NAVWEPS Report 8442, NOTS TP 3399), UNCLASSIFIED.

ABSTRACT. A propeller design method that treats the blades as lifting surfaces has been developed and programmed on an IBM 7090 computer. The singularity distributions representing the bound

(Over)
1 card, 4 copies

NAVWEPS Report 8442

circulation, shed vorticity, and blade thickness are treated as continuous sheets, making it necessary to determine the Cauchy principal value of the improper integrals expressing the induced velocities on the blades. The camber lines and pitch angles are determined from the variation of the normal component of induced velocity across the blade. This method is applicable to moderately loaded, non-optimum, wake-adapted propellers with or without skew.

NAVWEPS Report 8442

circulation, shed vorticity, and blade thickness are treated as continuous sheets, making it necessary to determine the Cauchy principal value of the improper integrals expressing the induced velocities on the blades. The camber lines and pitch angles are determined from the variation of the normal component of induced velocity across the blade. This method is applicable to moderately loaded, non-optimum, wake-adapted propellers with or without skew.

NAVWEPS Report 8442

circulation, shed vorticity, and blade thickness are treated as continuous sheets, making it necessary to determine the Cauchy principal value of the improper integrals expressing the induced velocities on the blades. The camber lines and pitch angles are determined from the variation of the normal component of induced velocity across the blade. This method is applicable to moderately loaded, non-optimum, wake-adapted propellers with or without skew.

NAVWEPS Report 8442

circulation, shed vorticity, and blade thickness are treated as continuous sheets, making it necessary to determine the Cauchy principal value of the improper integrals expressing the induced velocities on the blades. The camber lines and pitch angles are determined from the variation of the normal component of induced velocity across the blade. This method is applicable to moderately loaded, non-optimum, wake-adapted propellers with or without skew.

2 Maritime Administration
  Division of Research (1)
  Division of Ship Design (1)
3 California Institute of Technology, Pasadena
  Prof. A. J. Acosta (1)
  Prof. M. S. Plesset (1)
  Prof. T. Y. Wu (1)
3 Convair, San Diego
  A. D. MacLellan (1)
  H. T. Brooke (1)
  R. H. Oversmith (1)
1 Davidson Laboratory, Stevens Institute of Technology, Hoboken, N.J. (J. P. Breslin)
1 Dynamics Developments, Inc., Oyster Bay, N. Y.
1 Electric Boat Division, General Dynamics Corporation, Groton, Conn. (Robert McCandliss)
1 Gibbs and Cox, Inc., New York City
2 Grumman Aircraft Engineering Corporation, Bethpage, N. Y.
  E. Baird (1)
  E. Bower (1)
1 Lockheed Aircraft Corporation, Missiles and Space Division, Palo Alto, Calif. (R. W. Kermeen)
1 Lockheed - California Company, Burbank (Hydrodynamics Research, K. E. Hodge)
1 Massachusetts Institute of Technology, Cambridge (Prof. M. A. Abkowitz, Department of Naval Architecture and Marine Engineering)
1 Ordnance Research Laboratory, Pennsylvania State University, University Park (Dr. G. F. Wislicenus)
1 Society of Naval Architects and Marine Engineers, New York City
3 Southwest Research Institute, Department of Mechanical Sciences, San Antonio
  Dr. H. N. Abramson(1)
  G. Ransleben (1)
  Editor, Applied Mechanics Review (1)
1 Stanford University, Stanford, Calif. (Department of Civil Engineering, Dr. E. Y. Hsu)
1 State University of Iowa, Iowa Institute of Hydraulic Research, Iowa City (Dr. L. Landweber)
1 The Boeing Company, Seattle (M. J. Turner)
1 The University of Michigan, Ann Arbor (Department of Naval Architecture, Prof. R. B. Couch)
1 University of California at Los Angeles (Department of Engineering, Dr. A. Powell)
1 University of Minnesota, St. Anthony Falls Hydraulic Laboratory, Minneapolis (Dr. L. G. Straub)
1 Webb Institute of Naval Architecture, Glen Cove, N. Y. (Technical Library)
1 Adm Exp Works, Haslar, Gosport, Hants, England (Superintendant, A. J. Vosper), via BuWeps (DSC)

1 Bassin d'Essais des Carenes, Paris XVe, France (Director, Vice Adm. Roger E. Brard), via BuWeps (DSC)
1 British Ship Research Association, Prince Consort House, London, England, (H. Lackenby), via BuWeps (DSC)
1 Canal de Esperiencias Hidrodinamicas, El Prardo, Madrid, Spain (Director, Sr. M. Acevedo y Campoamor), via BuWeps (DSC)
1 Det Norske Veritas, Oslo, Norway (Managing Director, Dr. G. Vedeler), via BuWeps (DSC)
2 Hamburgische Schiffbau-Versuchsanstalt, Bramfelder Strasse 164, Hamburg, Germany, via BuWeps (DSC)
  Dr. H. W. Lerbs (1)
  Dr. O. Grim (1)
1 Hydro-og Aerodynamisk Laboratorium, Lyngby, Denmark (Prof. Carl Prohaska), via BuWeps (DSC)
1 Institut de Recherches de la Construction Navale, Paris, France (Director General, Dr. J. Dieudonne), via BuWeps (DSC)
1 Institut für Schiffbau der Universitat Hamburg, Berliner Tor 21, Hamburg, Germany (Director, Prof. G. P. Weinblum), via BuWeps (DSC)
1 Instituto Nazionale per Studi ed Esperienze di Architettura Navale, via della Vasca Navale 89, Rome, Italy, via BuWeps (DSC)
1 National Council for Industrial Res, TNO, The Hague, Netherlands (Prof. Laurens Troost, Jr.), via BuWeps (DSC)
1 National Physical Laboratory, Feltham, Middlesex, England (Director, Ship Division, A. Silverleaf), via BuWeps (DSC)
1 National Research Council, Ottawa, Canada (E. S. Turner), via BuWeps (DSC)
1 Nederlandsch, Scheepsbouwkundig Proefstation, Wageningen, The Netherlands (Dr. J. D. van Manen), via BuWeps (DSC)
1 Office, Natl d'Etudes et de Recherches Aeronautiques, Chatillion, Paris, France (Dr. L. Malavard, via BuWeps (DSC)
1 Skipsmodelltanken, Trondheim, Norway (Prof. J. K. Lunde), via BuWeps (DSC)
1 Staten Skeppsprovningsanstalt, Goteborg c, Sweden (Director, Dr. Hans Edstrand), via BuWeps (DSC)
1 Technische Hogeschool, Institut voor Toegepaste, Wiskunde, Julianalaan, 132, Delft, Netherlands (Prof. R. Timman), via BuWeps (DSC)
1 Versuchsanstalt für Wasserbau und Schiffbau, Schleuseninsel im Tiergarten Berlin, Germany (Director, Dr. S. Schuster), via BuWeps (DSC)
1 William Denny & Bros. Ltd., Exper Tank, Leven Shipyard, Dumbarton, Scotland (W. P. Walker), via BuWeps (DSC)